FINE STRUCTURE AND STARK EFFECT MEASUREMENTS ON He^+

by

Heinz-Jürgen Beyer

Thesis submitted to the University of Stirling

for the degree of Doctor of Philosophy

Physics Department

University of Stirling

Stirling

1973

SUMMARY

Anticrossing signals between magnetic sublevels from S and D and from S and F have been investigated in the n=4 state of He^+. The anticrossing positions in the magnetic field are shifted by the electric field necessary to induce the signals. Extrapolation to zero electric field has been carried out, and the following fine structure separations have been derived from the crossing positions so obtained:

	present experiment	theory (Erickson)
$4^2S_{1/2} - 4^2D_{3/2}$	(20 145.3 ± 7.8) MHz	(20 142.85 ± 1.36) MHz
$4^2S_{1/2} - 4^2D_{5/2}$	(27 455.4 ± 7.4) MHz	(27 458.60 ± 1.36) MHz
$4^2S_{1/2} - 4^2F_{5/2}$	(27 435.7 ± 13.8) MHz	(27 446.99 ± 1.36) MHz
$4^2S_{1/2} - 4^2F_{7/2}$	(31 098.2 ± 10.5) MHz	(31 104.78 ± 1.36) MHz

From these measurements values of the Lamb shift separations for $j > 1/2$ can be derived for the first time in this state:

$4^2D_{5/2} - 4^2F_{5/2}$	(19.7 ± 20.0) MHz	(11.61 ± 1.92) MHz
$4^2P_{3/2} - 4^2D_{3/2}$	(34.4 ± 9.0) MHz	(37.19 ± 1.36) MHz

For the latter the present result for $S_{1/2} - D_{3/2}$ is combined with the separation $S_{1/2} - P_{3/2}$ of (20179.7 ± 1.2) MHz, measured by Jacobs et al.. Experimental errors represent about 99% confidence limits, theory 68%.

The shift of the anticrossing positions with the electric field allows investigation of the "Stark effect of the fine structure" at fields of fifty to a few hundred V/cm, a region inaccessible to spectroscopic investigations. Within the present accuracy of approximately 15 - 20% the quadratic Stark constants agree with calculations based on diagonalization of the energy matrix in crossed magnetic and electric fields.

In addition anticrossing signals have been observed in n=5, and "cascading anticrossings" 5S - 5G could be detected by their effect on the population of sublevels of n=4.

ACKNOWLEDGEMENTS

I wish to thank Professor H. Kleinpoppen for the support of this work and for his encouragement and continuous interest in the progress.

My thanks go also to the other members of the Physics Department for their assistance and useful discussions. I would like to mention two in particular: K.-J. Kollath took part in numerous discussions and contributed many valuable suggestions in all stages of the investigation. He also came to help whenever two hands were not enough to cope with the apparatus. J.M. Woolsey joined the group in 1970 and for some time worked at the same system. This led to a very fruitful cooperation and encouraged us to tackle problems togetner.

I also thank for technical assistance from the technical staff of the Physics Department and of the University's Shared Technical Service. The tricky problem of the glass system was admirably handled by Mr. T.P. Young from the glassblowing workshop.

This research was supported by a grant from the Science Research Council.

TABLE OF CONTENTS

1 INTRODUCTION

1.1 Fine structure

The discovery of the Lamb shift $2^2S_{1/2} - 2^2P_{1/2}$ in hydrogen by Lamb and Retherford in 1947[1] prompted a large number of experimental and theoretical investigations of the fine structure of hydrogenic systems. Interest was focussed on the Lamb shift intervals $S_{1/2} - P_{1/2}$ to test the quantum-electrodynamical (qed) theory and on the fine structure intervals $P_{1/2} - P_{3/2}$, from which the fine structure constant α can be derived which in turn is used as expansion parameter in the qed calculations. The most accurate measurements have been done on the n=2 state of H, but in recent years there was considerable interest to extend investigations to higher Z- and to higher n-values to provide information about uncalculated Z- and n-dependent terms.

Most investigations of the n=4 state of He^+ (including the present one) made use of the line HeII-4686 Å (21 335 cm^{-1}), and this line complex 4S,P,D,F→3S,P,D played an important role in the exploration of the fine structure of hydrogenic systems. High resolution measurements extend from 1916, when Paschen[2] first partly resolved the line and compared the result with Sommerfeld's theory, to the most recent investigations by Larson and Stanley (1967)[3] and by Berry and Roesler (1970)[4]. Even more recently the line has been used to determine the Rydberg constant[5]. In general, the fine structure separations of n=3 and n=4, derived from these studies, agree with the predictions of the qed theory, but the accuracy is limited to the %-range by the Doppler width of the components, which greatly exceeds the natural width[4]. Owing to the recoil energy in the electron

1 W.E. Lamb, Jr. and R.C. Retherford, Phys. Rev. 72, 241-243 (1947)
2 F. Paschen, Ann. Physik (Leipzig) 50, 901-940 (1916)
3 H.P. Larson and R.W. Stanley, J.O.S.A. 57, 1439-1449 (1967)
4 H.C. Berry and F.L. Roesler, Phys. Rev. A 1, 1504-1517 (1970)
5 E.G. Kessler, Jr., Phys. Rev. A 7, 408-415 (1973)

scattering process this is the case even when an atomic beam arrangement is used[3]. A further complication arises from differential Doppler displacements of the various components of the line complex when using a hollow cathode[6,4].

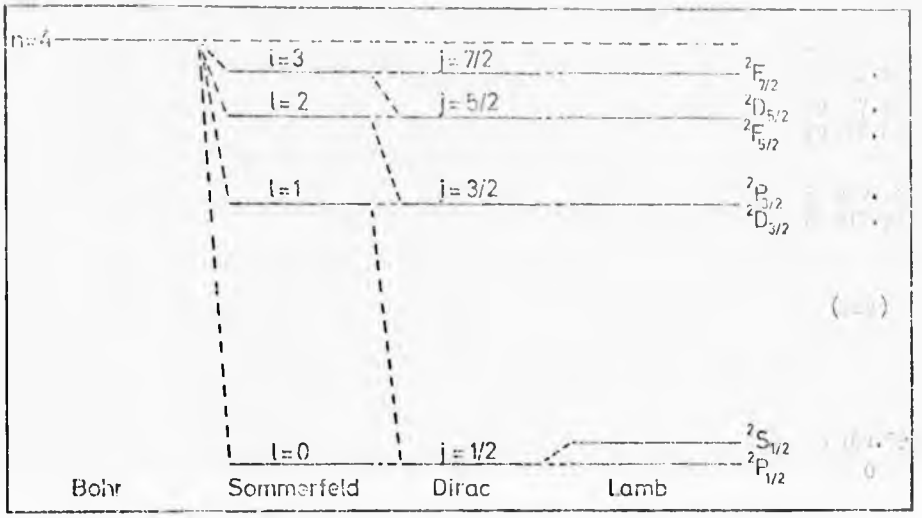

Fig. 1: Fine structure of the n=4 state of He^+. The noted energy values are calculated by Erickson[7]. The energy of $P_{1/2}$ is set zero.

Adopting radio frequency methods more accurate values have been obtained for the S-P intervals of n=4[8-11]. Anticrossing signals were also observed between magnetic sublevels of S and P[9], and Stark mixing effects were examined at and near such crossing points using high frequency modulated electron excitation[12,13].

6 F.L. Roesler and L. DeNoyer, Phys. Rev. Letters 12, 396-398 (1964)
7 G.W. Erickson, 1971, private communication
8 K.R. Lea, M. Leventhal, and W.E. Lamb, Jr., Phys. Rev. Letters 16, 163-165 (1966)
9 L.L. Hatfield and R.H. Hughes, Phys. Rev. 156, 102-108 (1967)
10 H.-J. Beyer and H. Kleinpoppen, Z. Physik 206, 177-183 (1967)
11 R.R. Jacobs, K.R. Lea, and W.E. Lamb, Jr., Phys. Rev. A 3, 884-905 (1971)
12 T. Hadeishi, Phys. Rev. Letters 21, 957-961 (1968)
13 T. Hadeishi, Phys. Rev. Letters 22, 815-816 (1969)

The other intervals of n=4 could not be investigated so easily, although radio frequency signals between P and D in n=3 of H had already been reported in 1960[14]. However, such signals are fairly weak and broad, and only recently have more detailed investigations been carried out comprising levels up to $F_{7/2}$ in n=3 to n=5 of H[15,16] and intervals P-D in n=3 of He^+[17]. Both, radio frequency[15,17] and anticrossing[16,17] signals were used to do this.

Another way to study levels with $l > 1$ was discovered by Eck and Huff[18]. In 1968 they reported direct anticrossing signals in He^+ between magnetic sublevels of 4S and 4D ($\Delta l = 2$) and of 4S and 4F ($\Delta l = 3$). Such higher order anticrossing signals are stronger and narrower than the corresponding P-D or D-F signals and are therefore better suited for accurate measurements.

The present experiment is based on these higher order anticrossing signals[19]. Improved experimental values are obtained for the energies of the D and F levels of n=4 of He^+, and these are used to derive for the first time measured values for the Lamb shift intervals $4^2P_{3/2} - 4^2D_{3/2}$ and $4^2D_{5/2} - 4^2F_{5/2}$. This report also gives a brief account of similar anticrossing signals in n=5 of He^+, detected in the line 3203 Å (n=5 → n=3), and of "cascading anticrossings" 5S-5G, detected in the line 4686 Å by their effect on the population of sublevels of n=4.

---

14 L.R. Wilcox and W.E. Lamb, Jr., Phys. Rev. 119, 1915-1933 (1960)
15 C.W. Fabjan, F.M. Pipkin, and M. Silverman, Phys. Rev. Letters 26, 347-350 (1971)
16 M. Glass-Maujean and J.-P. Descoubes, C.R. Acad. Sc. (Paris) 273, B-721-724 (1971)
17 A. Eibofner, Z. Physik 249, 58-72 (1971)
18 a) T.G. Eck and R.J. Huff, Beam Foil Spectroscopy, Ed. S. Bashkin (New York: Gordon and Breach, 1968), pp. 193-202
b) ---- Phys. Rev. Letters 22, 319-321 (1969)
19 Similar experiments on S-D anticrossings in hydrogen are being carried out by M. Glass-Maujean, T. Dohnalik, and J.-P. Descoubes, 1972, private communication

1.2 Stark effect

Much effort has been made to carry out precision measurements of the Stark effect in one-electron systems, which are best suited for comparison with theory. Canal rays were employed, and the splitting of hydrogen lines in an electric field was observed spectroscopically. Recently such an experiment has been done by Gebauer and Selhofer[20] on the H_β and H_γ lines of hydrogen. Good agreement with theory is reported for all electric fields used (upwards from 35 and 17 kV/cm for H_β and H_γ respectively). When the field strength is reduced further, spectroscopic investigations become difficult to perform, and below 20 kV/cm for H_γ there was some disagreement between theory[21] and experimental results from Steubing and Junge[22], who in particular observed no splitting at all below 2 kV/cm. However, more recent measurements[23,24] restored agreement with theory down to the lowest field strength, for which data could be taken (1.7 kV/cm).

In all investigations mentioned so far the pure linear Stark effect is predicted and observed[25]. If the field strength is reduced even further until the Stark splitting becomes comparable and then even small compared with the separations of interacting fine structure levels, the linear Stark effect changes over into the quadratic Stark effect. Following Rojansky[26] the term "Stark effect of the fine structure" is applied to this region. However, the fine structure separations in hydrogenic

20 R. Gebauer and H. Selhofer, Acta Phys. Austr. 31, 8-17 (1970) further reference to previous work may be found there
21 G. Lüders, Ann. Physik (6) 8, 301-321 (1951)
22 W. Steubing and W. Junge, Ann. Physik (6) 5, 108-116 (1949)
23 H. Rother, Ann. Physik (6) 17, 185-198 (1956)
24 R. Gebauer and H. Selhofer, Acta Phys. Austr. 31, 131-146 (1970)
25 Interactions with states with different principal quantum number n result in very small quadratic contributions in addition to the linear splitting. These are negligible at the low electric fields under consideration here because of the large energy separations to these states.
26 V. Rojansky, Phys. Rev. 33, 1 (1929)

systems are so small, that Stark effects of similar let alone much smaller size could not be observed spectroscopically.

In complex atoms the level crossing technique has been applied successfully to measure the quadratic Stark effect[27], which in turn is often used to test theoretical wavefunctions of these atoms. However, the application of this method to hydrogenic systems presents considerable experimental problems, since all resonance lines are in the vacuum ultraviolet, and the hydrogenic systems have to be produced first by dissociation (H, D) or by ionization (He,...)[28].

For these reasons there exist only very few investigations of the quadratic Stark effect in hydrogenic systems. The electric field dependence of the hyperfine interval of the ground state of H was derived from the frequency change of a hydrogen maser in an electric field[29,30]. Some investigation of the Stark effect of the fine structure was made possible with beam foil excitation: Intensity beats of the spectral lines were observed upon application of a static electric field[31], which couples fine structure levels with $\Delta l = \pm 1$. The beat frequency represents the corresponding fine structure separation and thus varies with the electric field. In n=2 of H the conditions are such that only the Lamb shift interval and

27 see for instance the review article by A.M. Bonch-Bruevich and V.A. Khodovoi, Usp. Fiz. Nauk 93, 71-110 (1967). Translation: Soviet Physics Uspekhi 10, 637-657 (1967/68)

28 Baird et al. performed a level crossing experiment on H, n=2, for a precision measurement of the fine structure constant α. A gas discharge was used to produce hydrogen atoms, and no Stark shift of the signal could be observed when a static electric field was introduced parallel to the magnetic field, a result of plasma screening.
J.C. Baird, J. Brandenberger, K.-I. Gondaira, and H. Metcalf, Phys. Rev. A 5, 564-587 (1972)

29 E.N. Fortson, D. Kleppner, and N.F. Ramsey, Phys. Rev. Letters 13, 22-25 (1964)

30 P.C. Gibbons and N.F. Ramsey, Phys. Rev. A 5, 73-78 (1972)

31 S. Bashkin, W.S. Bickel, D. Fink, and R.K. Wangsness, Phys. Rev. Letters 15, 284-285 (1965)

its variation with the electric field is detected[32-34]. The most recent investigation[33] was done for a field range from 100 to 400 V/cm and produced agreement with theory. The analysis of measurements at $n > 2$ in H^{+}[34,35] and He^{+}[36] is somewhat complicated because of the large number of possible beat frequencies.

A further way to study the Stark effect of the fine structure is provided by the anticrossing technique used in this work. A static electric field is required to induce the anticrossing signals and at the same time causes a Stark shift of the crossing position. There is also broadening and saturation of the signal with increasing electric field. First order anticrossing signals with $\Delta l = \pm 1$ like S-P need little electric field to be induced and become saturated and very broad before they show an appreciable shift. Hence no Stark shift had been observed in these signals. Higher order signals however, like S-D or S-F, require stronger electric fields to become visible and can be observed and analysed over a wider field range (between about fifty and a few hundred V/cm in the present experiment). Stark shifts then become very apparent and allow investigation of the Stark effect of the fine structure.

32 I.A. Sellin, C.D. Moak, P.M. Griffin, and J.A. Biggerstaff, Phys. Rev. 188, 217-221 (1969)
33 H.J. Andrä, Phys. Rev. A 2, 2200-2207 (1970)
34 W.S. Bickel, J.O.S.A. 58, 213-221 (1968)
35 I.A. Sellin, C.D. Moak, P.M. Griffin, and J.A. Biggerstaff, Phys. Rev. 184, 56-63 (1969)
36 W.S. Bickel and S. Bashkin, Phys. Rev. 162, 12-15 (1967)

2 BASIS OF THE EXPERIMENT

An unmodulated beam of electrons is used to produce excited helium ions in an atmosphere of about 10^{-2} Torr of helium. At energies of the order of 300 eV the dominating excitation process is simultaneous ionization and excitation of ground state helium atoms[37] with some additional cascading effects[38]. Adopting rectangular coordinates x, y, z, the intensity of the unresolved line complex n=4 → n=3 at 4686 Å is recorded in y-direction. A magnetic field is applied in z-direction parallel to the electron beam, and a static electric field in ±x-direction. In an appropriate electric field and on variation of the magnetic field through the crossing position of suitable sublevels of n=4, state mixing between these sublevels occurs causing a change of the population equilibrium which in turn alters intensity and polarization of the line 4686 Å. As a result of the state mixing the sublevels repell each other so that the actual crossing is removed. For this reason such signals are called anti-crossings.

Basically anticrossing signals are equivalent to the more familiar electric radio frequency transitions - at zero frequency: An electric field (rf when the levels are separated, dc when they cross) is applied to mix the two levels of interest, and a resonance signal can be observed, provided the undisturbed levels had different populations and the change of population can be detected.

Using electron excitation in low pressure helium, the sublevels of S, P, D, and F are not equally populated under steady state conditions because of both, different cross sections[37] and different lifetimes[39]. In particular S-sublevels are strongly populated whereas the population of sublevels from P, D, and F states as well as the population differences

37 R.J. Anderson, E.F.P. Lee, and C.C. Lin, Phys. Rev. 160, 20-23 (1967)
38 R.J. Anderson and R.H. Hughes, Phys. Rev. A 5, 1194-1197 (1972)
39 F.L. Roesler and J.E. Mack, Phys. Rev. 135, A56-A71 (1964)

between them are much smaller - one reason for signals P-D and D-F (mentioned in 1.1) being weaker than signals involving S.

state	4S	4P	4D	4F
lifetime (10^{-8}s)	1.4154	0.07667	0.2258	0.4551

Table 1: Calculated lifetimes for the n=4 state of He^+ [39]

Consider now two suitable sublevels of n=4 at and near their crossing point in the magnetic field. Without coupling (electric field off) the sublevels decay undisturbed with their characteristic lifetimes and according to the branching ratios shown in Fig. 2. From the different spectral lines radiated on decay from n=4, only the line complex 4686 Å is detected, corresponding to all components of the direct decay n=4 → n=3. If the electric field is switched on, state mixing occurs at and near the

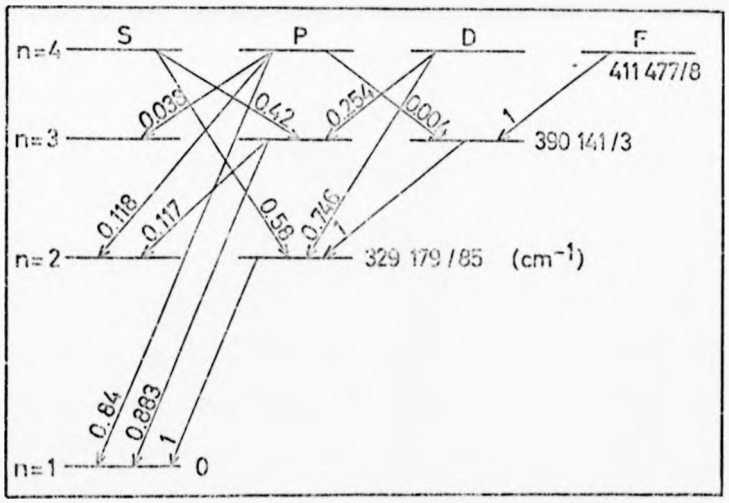

Fig. 2: Branching ratios for one-electron systems. The numbers at the arrows show the relative probability for an excited state to decay through this channel. The energies are for He^+ and not drawn to scale. Ref. 40, Sect. 63.

40 H.A. Bethe and E.E. Salpeter, Quantum Mechanics of One- and Two-Electron Atoms (Berlin: Springer Verlag, 1957)

crossing point, equivalent to induced transitions from the more to the less populated sublevel. Taking an anticrossing between sublevels from S and P as example, this results in less decay through 4S and more decay through 4P. It follows from Fig. 2 that 30% of the net transitions 4S → 4P are detected as intensity loss of the line n=4 → n=3. Similarly, for anticrossings 4S-4D there is a loss of 17% of the net transitions and for 4S-4F a gain of 58%. The decay of all other sublevels ideally remains unchanged giving rise only to a constant background.

This general picture is modified if sublevels with non-spherical symmetry are involved. In these cases polarization effects can have considerable influence on the actual signal strength (→5.2). Furthermore the shape of S-D signals is changed under certain circumstances by interference effects in the decay channel (→3.1.3).

3 THEORETICAL CONSIDERATIONS

All numerical results are based on Erickson's[7] energy values for one-electron systems shown in Fig. 1 for n=4 of He^+, the lifetimes given in Table 1, and the fundamental constants from Taylor et al.[41].

3.1 Crossing signals

The possibility of observing signals at and near the crossing position of two levels with different parity has been discussed by Series[42] for the case of one of the levels having infinite lifetime. Wieder and Eck[43] later derived a general equation for crossing signals. This formula is copied in Appendix 1. The calculation assumes light excitation, but the essential features are the same when electron excitation is used.

Apart from a non-resonant background (parts 1 and 2 of the equation) 3 groups of processes contribute to the signal:

a) pure level crossing processes (parts 3 and 4)

b) pure anticrossing processes (part 5)

c) processes combining characteristics from a) and b) (parts 6-8)

3.1.1 Level crossing signals

Level crossing signals of type a) are the result of a redistribution of the radiation near the crossing point. Basically this is an interference effect[44,45] and, in order to obtain a signal, coherent excitation of the

41 B.N. Taylor, W.H. Parker, and D.N. Langenberg, Revs. Mod. Phys. 41, 375-496 (1969)
42 G.W. Series, Phys. Rev. 136, A684-A688 (1964)
43 H. Wieder and T.G. Eck, Phys. Rev. 153, 103-112 (1967)
44 F.D. Colegrove, P.A. Franken, R.R. Lewis, and R.H. Sands, Phys. Rev. Letters 3, 420-422 (1959)
45 P.A. Franken, Phys. Rev. 121, 508-512 (1961)

two crossing levels is required and at least partial decay to a common lower level, in resonance fluorescence usually excitation from and decay to common levels. Selection rules follow from these conditions.

3.1.2 Anticrossing signals

Pure anticrossing signals of type b) form the basis of the present investigation as outlined in Chapter 2. No interference effects are involved here. The signal is described by part 5 of the equation from Wieder and Eck[43] (→Appendix 1), which is identical with the expression obtained by Lamb and Sanders[46] for electric dipole radio frequency transitions, if only the resonant component of the radio frequency field is accounted for. The expected anticrossing signal in dependence of the separation $\Delta\nu$ of the undisturbed sublevels a and b represents an absorption Lorentzian curve centred at $\Delta\nu = 0$:

$$S(\Delta\nu) = \frac{A}{1 + \Delta\nu^2/B^2} \tag{1}$$

with the amplitude A and the full width at half maximum 2B:

$$A = -\frac{(f_a - f_b)(r_a/\gamma_a - r_b/\gamma_b)\ |2V_{ab}|^2}{(\gamma_a + \gamma_b)(1 + |2V_{ab}|^2/\gamma_a\gamma_b)} \tag{2}$$

$$2B = (\gamma_a + \gamma_b)\sqrt{1 + |2V_{ab}|^2/\gamma_a\gamma_b} \tag{3}$$

$(f_a - f_b)$ is the difference of the branching ratios. $(r_a/\gamma_a - r_b/\gamma_b)$ is the steady state population difference of levels a and b, where r_a, r_b are the excitation rates and γ_a, γ_b the natural level widths in frequency units ($\gamma = 1/2\pi\tau$, τ lifetime). V_{ab} is the interaction element between

46 W.E. Lamb, Jr. and T.M. Sanders, Phys. Rev. 119, 1901-1914 (1960)

a and b. For electric dipole coupling ($\Delta l = 1$) induced by an electric field $\vec{F}$ it is:

$$V_{ab} = \frac{1}{h} \vec{F} \langle a | e\vec{r} | b \rangle \tag{4}$$

There is no signal without electric field ($V_{ab} = 0$). With increasing field the signal amplitude at first rises proportional to $|V_{ab}|^2$. Then the rise slows down and for large $|V_{ab}|$ the signal becomes saturated. The signal width, starting from the sum of the natural widths $\gamma_a + \gamma_b$, increases continuously with the electric field.

50% saturation of the signal is reached for:

$$|V_{ab}|_{50\%} = \frac{1}{2}\sqrt{\gamma_a \gamma_b} \tag{5}$$

with a corresponding width of:

$$2B_{50\%} = \sqrt{2}\,(\gamma_a + \gamma_b) \tag{6}$$

For small electric field, coupling will be restricted to states with $\Delta l = 1$, for which V_{ab} is given by (4). However, in hydrogenic fine structure systems like n=4 of He^+ with many sublevels almost degenerate, an increasing electric field will soon also induce noticeable higher order Stark mixing, and higher order anticrossing signals with $\Delta l = 2, 3, \ldots$ become observable. This higher order coupling is achieved through one or more intermediate states, each step being governed by the appropriate dipole selection rules since a homogeneous electric field can only produce electric dipole coupling. Usually several channels are open to connect a and b, and the sum over all possible intermediate states has to be taken to evaluate V_{ab}[47]. For a and b belonging to S ($l = 0$) and F ($l = 3$) respectively, the lowest order interaction element would be of the form:

47 Again states with different principal quantum number n can be disregarded because of their large energy separation as compared to states within the same fine structure system.

$$V_{ab} \propto \sum_{\substack{i \\ l=1}} \sum_{\substack{j \\ l=2}} \langle a|e\vec{F}\cdot\vec{r}|i\rangle \langle i|e\vec{F}\cdot\vec{r}|j\rangle \langle j|e\vec{F}\cdot\vec{r}|b\rangle \propto |\vec{F}|^3 \qquad (7)$$

with various energy separations in the denominator.

If one such channel dominates the interaction between a and b, the coupling may be approximated by a 3-level system for anticrossings with $\Delta l = 2$ and by a 4-level system for $\Delta l = 3$. On this basis Glass-Maujean and Descoubes[48] calculated one anticrossing signal S-D for n=4 of hydrogen. Their (numerical) results, apart from displaying the features discussed above, also show a Stark shift of the crossing position if the electric field interaction with the intermediate state is different for a and b. However, a number of further sublevels, having little or no influence on the coupling of a and b, still contributes to the Stark shift of the crossing position. Sublevels excluded might also give rise to signal asymmetries. Hence the 3- or 4-level model can neither give the accurate crossing position nor the correct signal form. Apart from that, the signal amplitude can hardly be calculated anyway owing to the lack of knowledge of the excitation cross sections of the various sublevels.

In 3.2.3 the crossing positions are calculated independently of the theory of the anticrossing signals. Nevertheless, this calculation provides important information on the anticrossing signal and allows to check the assumption made above of a multistep dipole coupling process (→3.3 and 6.1).

48 M. Glass-Maujean and J.-P. Descoubes, Optics Comm. 4, 345-351 (1972)

3.1.3 Mixed level- and anticrossing signals

For anticrossing signals between sublevels with $\Delta l = 2$ (S-D in this experiment) processes of type c) of the list in 3.1 are possible in addition to the pure anticrossing signals of type b).

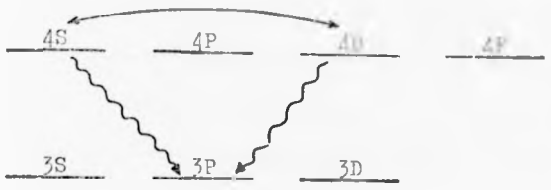

Fig. 3: Basis for mixed level- and anti-crossing signals (see text)

Fig. 3 shows schematically that in this case decay is allowed from both crossing sublevels to a common sublevel in n=3. If the sublevels were excited coherently, a level crossing signal of type a) should be observable without application of an electric field. This has not been detected, but coherence is introduced by the mixing electric field, giving rise to interference effects in the decay channel. Parts 7 and 8 of the equation of Wieder and Eck[43] (→Appendix 1) take account of such effects. Part 7 in particular, being of dispersion shape, results in a distortion of the original absorption type signal.

The interference term has also been obtained by Glass-Maujean and Descoubes[48] in their calculation of the S-D anticrossing signal in n=4 of hydrogen (→3.1.2).

The interference part of the signal can be excluded if the observation conditions are chosen in such a way that no decay exists to common sublevels, in the present set-up by selecting π-light for the detection. However, this tends to reduce the signal, so that the analysis of the mixed structure is usually preferable.

3.2 Zeeman and Stark effects

3.2.1 Introduction

Anticrossing signals are observed if an appropriate magnetic field is applied to cross suitable sublevels and an electric field added to couple them. The influence of the electric field on the sublevel energies, though small, is not negligible as the Stark shift of the anticrossing signals shows. It is therefore necessary for the experimental determination of the fine structure separations to extrapolate the crossing positions to zero electric field before applying the Zeeman theory to calculate back to zero magnetic field. For a better comparison, and in particular for the analysis of the Stark effect, the theoretical crossing positions have to be calculated with both fields applied.

This is done in two ways. In 3.2.2 an independent treatment of Zeeman and Stark effect is described. This provides a good approximation for low electric field. Accurate results for all fields likely to be encountered are obtained from numerical diagonalization of the energy matrix of n=4 in combined electric and magnetic fields. This is described in 3.2.3.

3.2.2 Independent treatment of Zeeman and Stark effects

The splitting of the fine structure system n=4 of He^+ in a magnetic field alone is calculated from equation 46.15 of Bethe and Salpeter[40], incorporating the influences of the nuclear motion (Ref. 40, 47β) and of the anomalous magnetic moment of the electron (Ref. 40, 47ε). This is shown in Fig. 4.

A small electric field has little influence on the energy of the magnetic sublevels. Therefore only contributions are considered from those sublevels which couple directly with either of the crossing sublevels by

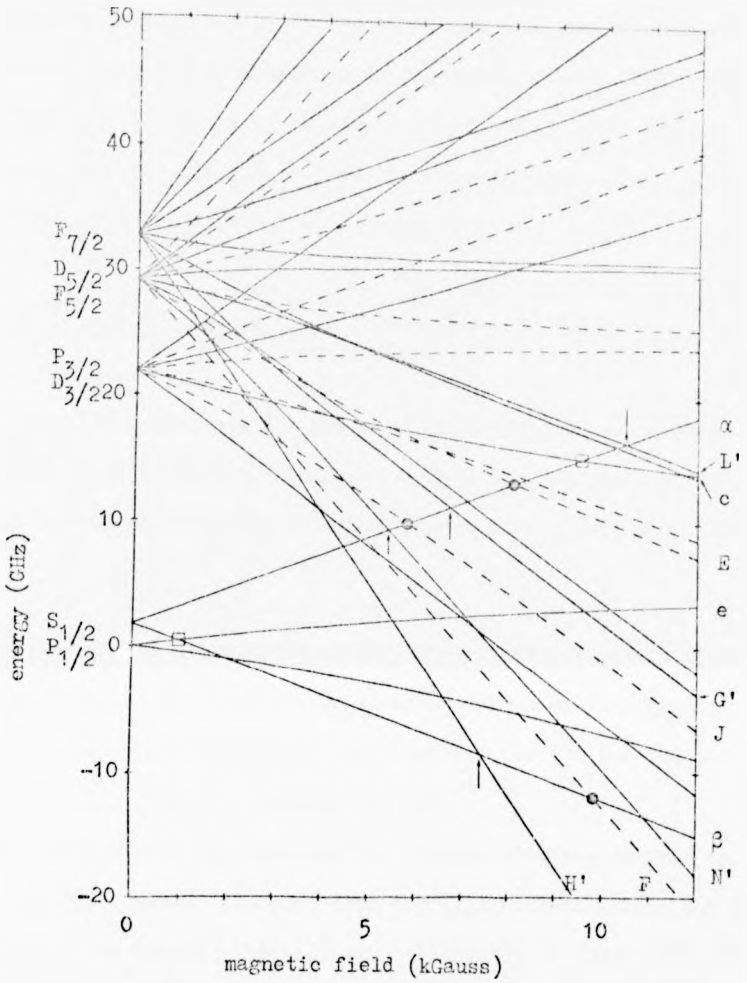

Fig. 4 (Fig. 3 of Ref. 18a): Zeeman effect of the fine structure system n=4 of He^+. The D sublevels are shown as dashed lines, the others as solid lines. Anticrossings occuring between sublevels from S and sublevels from P, D, and F (on application of an electric field perpendicular to the magnetic field) are marked by squares, circles, and arrows respectively. Lamb's notation of the sublevels is used. It is explained in Appendix 2.

dipole interaction. This rejection of multistep processes separates the system into independent 2-level systems and thus greatly reduces the number of sublevels contributing to the shift of each anticrossing. Hence the overall Stark displacement of a magnetic sublevel a with energy E_a in an electric field $\vec{F}$ is given by the sum of the contributions from all interacting sublevels m with energy E_m:

$$E - E_a = \frac{1}{2} \sum_m (E_a - E_m) \left\{ \sqrt{1 + \frac{4|V_{am}|^2}{(E_a - E_m)^2}} - 1 \right\} \qquad (8)$$

This equation represents the exact solution for 2-level systems.

Taking the magnetic field along the z-direction and the electric field along the x-direction, the interaction element V_{am} becomes:

$$V_{am} = F_x \langle a|ex|m \rangle \qquad (9)$$

$\langle a|ex|m \rangle$ is the x-component of the electric dipole matrix element connecting a and m. These matrix elements depend on the magnetic field, and the appropriate values are computed from Pauli eigenfunctions in the magnetic field (Ref. 40, equation 46.17).

The Stark shifts of the anticrossing signals obtained in this way are shown in Figs. 21 - 25 together with the experimental shifts and the results of the matrix diagonalization (→3.2.3). A comparison indicates that in n=4 of He^+ this approach usually represents a good approximation for electric fields below about 150 V/cm.

3.2.3 Combined treatment of Zeeman and Stark effects
(matrix diagonalization)

The treatment described in 3.2.2 is no more appropriate when the electric field is large enough to produce an appreciable contribution from higher order Stark effect (breakdown of the 2-level approach) and when the Stark energies become comparable with the Zeeman energies. The general problem is solved by diagonalizing the energy matrix of the full system (32×32 for n=4), applying electric and magnetic fields simultaneously.

3.2.3.1 Setting up the matrix

The matrix is set up in the high field n,l,m_l,m_s-representation[49] (Paschen-Back effect). The effective Hamiltonian is:

$$H = H^I + H^M + H^F \qquad (10)$$

where H^I, H^M, H^F represent the spin-orbit, the magnetic field, and the electric field (dipole) interaction respectively. H^I and H^M couple states with $\Delta l = 0$, whereas H^F requires a change of parity, $\Delta l = \pm 1$, to have elements different from zero. In the high field representation H^M is diagonal, and H^I contains diagonal and off-diagonal elements. Diagonalization of H^I alone provides the fine structure energies in zero field. For the present calculations however, these energy values are taken from Erickson[7] and incorporated into the matrix in order to include the important qed corrections.

49 E.U. Condon and G.H. Shortley, The Theory of Atomic Spectra (London: Cambridge University Press, 1970), Chapter V

The matrix elements of $H^I + H^M$ are therefore ($m = m_l + m_s$):

$$\langle n\, l\, m_s\, m_l | H^I + H^M | n\, l\, m_s'\, m_l' \rangle = \langle n\, l\, m_s'\, m_l' | H^I + H^M | n\, l\, m_s\, m_l \rangle$$

$$= \left\{ W_{j=l-1/2} + \frac{\Delta W}{2l+1}(l+1+2m_l m_s) + \mu_B H(g_l m_l + g_s m_s) \right\} \delta_{m_s m_s'} \delta_{m_l m_l'} \qquad (11)$$

$$+ \frac{\Delta W}{2l+1} \sqrt{(l-m+1/2)(l+m+1/2)}\ \delta_{m_s' m_s \pm 1} \delta_{m_l' m_l \mp 1}$$

$W_{j=l-1/2}$ is the zero field energy of the fine structure level with $j=l-1/2$. ΔW is the fine structure separation $W_{j=l+1/2} - W_{j=l-1/2}$ in zero field. μ_B is Bohrs magneton, H the magnetic field taken in z-direction. g_l includes the correction for the nuclear motion:

$g_l = 1 - m/M$ (m: electron mass, M: mass of the nucleus)

$g_s = 2\,\mu_e/\mu_B$ (μ_e: magnetic moment of the electron)

The effective Hamiltonian H^F is:

$$H^F = e\vec{F}\cdot\vec{r} \qquad (12)$$

$\vec{F}$ is assumed to be in the z-x-plane and is split up into the two components F_z (parallel to H) and F_x (perpendicular to H). Using the eigenfunctions $4^5 2$ from Condon and Shortley[49], the non-zero matrix elements of H^F are obtained (a_o: Bohrs radius):

$$\langle n\, l+1\, m_l'\, m_s | e\vec{F}\cdot\vec{r} | n\, l\, m_l\, m_s \rangle = \langle n\, l\, m_l\, m_s | e\vec{F}\cdot\vec{r} | n\, l+1\, m_l'\, m_s \rangle$$

$$= \frac{3}{2}\frac{n}{Z}\sqrt{n^2-(l+1)^2}\ \sqrt{\frac{(l-m_l+1)(l+m_l+1)}{(2l+1)(2l+3)}}\ \delta_{m_l m_l'}\, e a_o F_z \qquad (13)$$

$$\mp \frac{3}{4}\frac{n}{Z}\sqrt{n^2-(l+1)^2}\ \sqrt{\frac{(l\pm m_l+1)(l\pm m_l+2)}{(2l+1)(2l+3)}}\ \delta_{m_l' m_l \pm 1}\, e a_o F_x$$

Computer subroutines have been set up to calculate the matrix for any combination of magnetic and electric fields. This is done in a general way for all one-electron fine structure systems.

3.2.3.2 Diagonalization of the matrix[50]

Householders method[51] is used to reduce the matrix to a triple diagonal matrix which has the same eigenvalues. These are found by a bisection method based on a Sturm sequence[52]. The eigenvectors of the triple diagonal matrix are found by inverse iteration[53], and these are transformed to the eigenvectors of the original matrix[51]. The eigenvalues and the corresponding eigenvectors are printed in ascending order. Another subroutine evaluates the crossing or anticrossing position (the latter is taken to be the point of minimum separation of the two sublevels under consideration). The results thus obtained are compared with the measurements in Figs. 21-25 in 6.2.

3.2.4 Crossing points in magnetic and electric fields

In a magnetic field alone, a level system like n=4 of He^+ splits into sublevels with a number of crossing points at intermediate field strength as shown in Fig. 4. Crossings between sublevels with $\Delta l = \Delta m_j = 0$ ($m_j = m_l + m_s$) are suppressed because these are coupled by the magnetic field and thus repell each other. An electric field on the other hand couples levels with different l-values, $\Delta l = \pm 1$ for dipole coupling in a homogeneous electric field.

Simultaneous application of magnetic and electric fields removes all crossovers in accordance with the von Neumann-Wigner "no crossing

50 The diagonalization programme has been set up by J.M. Woolsey, who did such calculations on the basis of the low field n,l,j,m_j-representation. His results are confirmed.
51 J.H. Wilkinson, Numerische Mathematik 4, 354-361 (1962)
52 W. Barth, R.S. Martin, and J.H. Wilkinson, Numerische Mathematik 9, 386-393 (1967)
53 J.H. Wilkinson, Numerische Mathematik 4, 368-376 (1962)

3.2.3.2 Diagonalization of the matrix[50]

Householders method[51] is used to reduce the matrix to a triple diagonal matrix which has the same eigenvalues. These are found by a bisection method based on a Sturm sequence[52]. The eigenvectors of the triple diagonal matrix are found by inverse iteration[53], and these are transformed to the eigenvectors of the original matrix[51]. The eigenvalues and the corresponding eigenvectors are printed in ascending order. Another subroutine evaluates the crossing or anticrossing position (the latter is taken to be the point of minimum separation of the two sublevels under consideration). The results thus obtained are compared with the measurements in Figs. 21-25 in 6.2.

3.2.4 Crossing points in magnetic and electric fields

In a magnetic field alone, a level system like n=4 of He^+ splits into sublevels with a number of crossing points at intermediate field strength as shown in Fig. 4. Crossings between sublevels with $\Delta l = \Delta m_j = 0$ ($m_j = m_l + m_s$) are suppressed because these are coupled by the magnetic field and thus repell each other. An electric field on the other hand couples levels with different l-values, $\Delta l = \pm 1$ for dipole coupling in a homogeneous electric field.

Simultaneous application of magnetic and electric fields removes all crossovers in accordance with the von Neumann-Wigner "no crossing

50 The diagonalization programme has been set up by J.M. Woolsey, who did such calculations on the basis of the low field n,l,j,m_j-representation. His results are confirmed.
51 J.H. Wilkinson, Numerische Mathematik 4, 354-361 (1962)
52 W. Barth, R.S. Martin, and J.H. Wilkinson, Numerische Mathematik 9, 386-393 (1967)
53 J.H. Wilkinson, Numerische Mathematik 4, 368-376 (1962)

theorem"[54], provided the electric field is neither parallel nor perpendicular to the magnetic field. For $\vec{H} \parallel \vec{F}$ sublevels with different m_j might still cross, and for $\vec{H} \perp \vec{F}$ crossings may occur between sublevels with $l + m_j + 1/2$ even and $l + m_j + 1/2$ odd. Since only electric dipole interaction elements have been included in the matrix, this implies multistep dipole coupling to bridge $\Delta l = 2$ and 3. The calculated eigenvalues prove that such coupling indeed exists, and the eigenvectors show an admixture of intermediate states. Fig. 5 shows the calculated energies of sublevels α ($l = 0$) and G' ($l = 3$) near their crossing for various electric field values ($\vec{F} \perp \vec{H}$). In the electric field the actual crossing is removed, and at the same time an anticrossing signal can be detected.

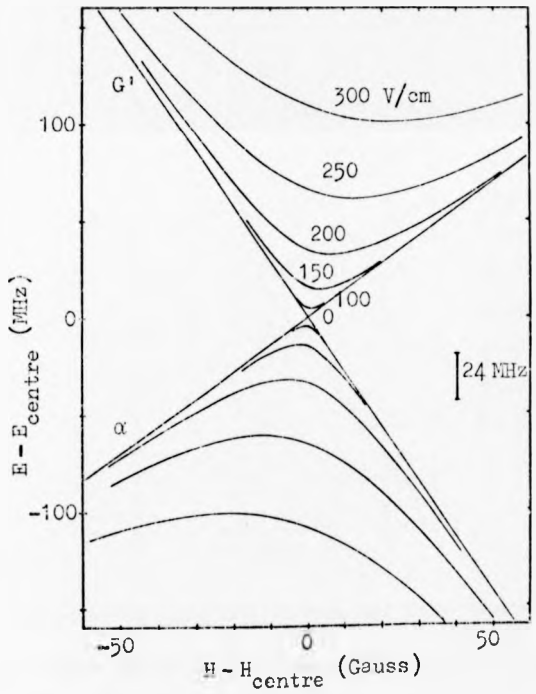

Fig. 5: Eigenvalues of the sublevels α and G' of n=4 of He^+ near their crossing position for various electric field strengths ($\vec{F} \perp \vec{H}$), calculated from time independent matrix diagonalization. The crossing centre is normalized to a common position (E_o, H_o) for all electric fields. The separation of the eigenvalues at H_o represents $2|V_{\alpha G'}| \cdot \gamma_\alpha - \gamma_{G'} = 24$ MHz is marked by the bar. Near the crossing the time dependent results would depart strongly (producing a real crossing) for $2|V_{\alpha G'}| \leq 12$ MHz and show little change for $2|V_{\alpha G'}| > 24$ MHz.

54 J. von Neumann and E. Wigner, Physik. Z. 30, 467-469 (1929)

It will be verified quantitatively in 3.3 that this coupling process is responsible for the observed anticrossing signals. The above coupling rules for $\vec{H} \parallel \vec{F}$ and $\vec{H} \perp \vec{F}$ therefore represent selection rules for these signals.

For sublevels with different lifetimes, the time dependent theoretical approach should be used. At low electric field this would modify the energies of sublevels near crossing points. Lamb[55], Series[42], and Wieder and Eck[43] proved for simple systems that sublevels, supposed not to cross according to the time independent theory, still do cross when the electric field interaction energy is less than or equal to the energy corresponding to a quarter of the difference between the linewidths ($|V| \leq \frac{1}{4} |\gamma_a - \gamma_b|$). Fig. 6 shows the example given by Lamb[55].

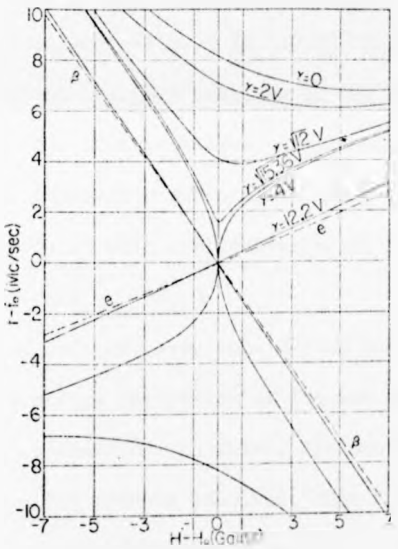

Fig. 6 (Fig. 51 from Ref. 55): Stark effect of two sublevels in time dependent theory for various ratios of the Stark interaction energy V to the difference of the linewidths γ. The example is for ^2H, n=2, sublevels β and e. $H_o = 575$ G, $F = 3.6$ V/cm, $\gamma_\beta = 0$, $\gamma_e = 100$ MHz.

The matrix diagonalization has been carried out in time independent theory and therefore cannot give these finer points. Anticrossing behaviour shows up independently of the lifetimes of the sublevels

55 W.E. Lamb, Jr., Phys. Rev. 85, 259-276 (1952)

as soon as an electric field interaction occurs. However, this has negligible effect on the calculated Stark shift of the present anticrossing signals since the shift is caused by sublevels separated by at least several level widths.

3.3 Anticrossing signals and matrix diagonalization

It has been pointed out in 3.1.2 that a closed calculation of higher order anticrossing signals would be difficult because of the many sublevels contributing to position and strength of the signal. The numerical matrix diagonalization, although carried out in the first place to obtain the correct crossing positions, has already proved that dipole coupling is sufficient to convert crossings of sublevels with $\Delta l > 1$ into anticrossings (→Fig. 5 in 3.2.4). Moreover it can now be verified that multistep dipole coupling of the lowest possible order is the dominant process to induce the observed anticrossing signals.

Two degenerate sublevels a and b (in time independent theory) become separated with application of an electric field by:

$$\Delta E_o = |2V_{ab}| \qquad (14)$$

Thus, without even considering details, V_{ab} can be deduced directly from the energy separation of the two eigenvalues at the crossing position as obtained by the matrix diagonalization. Provided there is no additional coupling process involved, this V_{ab} also governs the anticrossing signal (equations (1) to (3) in 3.1.2), so that the electric field dependent parts of the anticrossing signals can now be evaluated and compared with the experimental signals. In Fig. 7 the energy separation at the crossing position of sublevels α and α', taken from Fig. 5, is plotted directly as a function of the electric field. Within the used electric field range,

$V_{\alpha G'}$ follows a F_x^3-dependence as expected for S-F signals from equation (7) in 3.1.2.

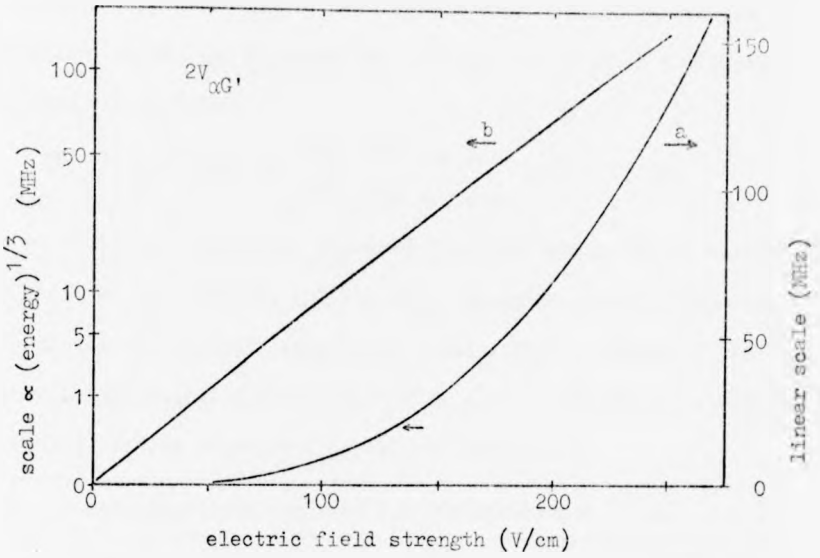

Fig. 7: Calculated electric field interaction energy $2|V_{\alpha G'}|$ at the crossing position of sublevels α and G' (H_o in Fig. 5) in dependence of the electric field strength. a: linear energy scale, b: expanded energy scale $\propto \sqrt[3]{\text{energy}}$, showing that $V_{\alpha G'} \propto F^3$ within the range used. 50% saturation of the anticrossing signal is expected according to equation (5) in 3.1.2 for $2|V_{\alpha G'}| = 19.8$ MHz, marked by an arrow.

The theoretical values for V_{ab} thus obtained are inserted into equations (2) and (3) of 3.1.2 to calculate the absolute signal width and the relative signal amplitude in dependence of the electric field. The amplitude remains relative because of the unknown excitation cross sections. In Fig. 20 of 6.1 the result of this calculation is compared with the measurement, again for the anticrossing $\alpha G'$. This shows very good agreement between theory and experiment.

A simpler test for all anticrossing signals observed in n=4 of He^+ is done in Table 2, comparing the theoretical and experimental electric fields for 50% saturation of the signals. The theoretical values are determined as in Fig. 7, using the lifetimes of Table 1 in Chapter 2 and equation (5) in 3.1.2:

$$2|V_{ab}|_{50\%} = \sqrt{\gamma_a \gamma_b} = \begin{matrix} 19.8 \text{ MHz for S-F} \\ 28.0 \text{ MHz for S-D} \end{matrix} \quad \text{in n=4 of } He^+$$

The experimental values are obtained firstly, taking 50% of the saturation amplitude of the signals, and secondly, applying equation (6) in 3.1.2 with the lifetimes again from Table 1 and with the slopes of the sublevels in the magnetic field as in Fig. 4 in 3.2.2. There is satisfactory agreement between theory and experiment throughout.

electric field required for 50% saturation (V/cm)					
anticrossing	S-F			S-D	
	αN'	αG'	βH'	αJ	αE
calculated	133	130.5	158.6	90	41
measured amplitude	133	131	153	75	39
measured width	101	125	133	78	34

Table 2: Comparison of the calculated and measured electric field strengths required for 50% saturation of the anticrossing signals observed in n=4 of He^+. The experimental results based on the signal width are less reliable than the data for 50% of the saturation amplitude, in particular when the signals are strongly shifted by the electric field (all but αG'): In this case the angle in the magnetic field between the crossing sublevels might change with the electric field, and furthermore the signals will be broadened by inhomogeneities of the electric field. Estimated uncertainties: For 50% of the saturation amplitude ~ ±10 V/cm, for the signal width ~ $^{-15}_{+35}$ V/cm, except αG': ±15 V/cm.

4 APPARATUS

4.1 General considerations

A new apparatus was built up for the present investigation. Four main areas of experimental technique and equipment had to be considered:

1) vacuum system and electron gun - light source (→4.2)
2) magnetic field and field measurement (→4.3)
3) application of a radio frequency field (→4.4)
4) light detection and signal recording (→4.5)

The basic equipment was carefully selected to allow for future precision experiments. On the other hand a high degree of flexibility was aimed at, not only to be able to cope with new developments, but also to fit the equipment into the general requirements of the experimental physics group just having been established.

A "preliminary" electron gun - light source (tube 1) was built to gain experience with the new system and to test the feasibility of fine structure measurements in n=5. It was not planned with tube 1 to introduce a radio frequency field (considered necessary for the intended Lamb shift measurement in n=5). Instead the opportunity was taken to incorporate two Stark plates for application of a static electric field and to look out for higher order anticrossing signals in n=4 and n=5, as they had been observed not long before in n=4 by Eck and Huff[18]. Tentative investigations of the anticrossing signals in n=4 soon revealed the possibility of determining the fine structure separations S-D and S-F with much better accuracy than before[18] and of measuring the Stark effect of the fine structure at the same time. The detailed investigation of n=5 was therefore postponed and priority given to the study of the anticrossing signals in n=4. All measurements in this report have been carried out

with tube 1. A block diagramme of the experimental arrangement is shown in Fig. 8.

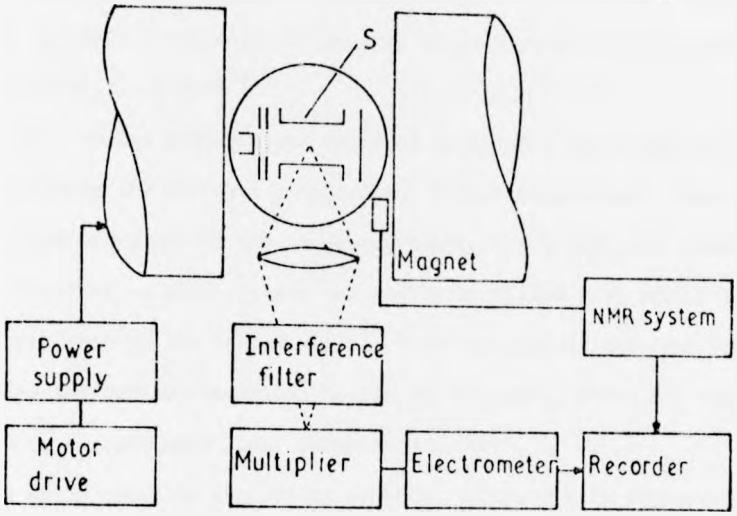

Fig. 8: Experimental arrangement. The glass vacuum system is sealed and contains the electron gun and approximately 10^{-2} Torr of helium. S: Stark plates for application of an electric field perpendicular to the magnetic field.

4.2 Vacuum system and electron gun

The electron gun in a low pressure helium atmosphere forms the heart of the system. Once the spectral lines for the observation have been chosen there are three main requirements to be fulfilled: (1) a stable helium pressure together with a low background pressure, (2) small dimensions along the electron beam to fit into the air gap of the magnet, and (3) no ferromagnetic materials.

Spectral lines for the detection can be selected from the lines 4686 Å ($n=4 \rightarrow n=3$) or 1215 Å ($n=4 \rightarrow n=2$) for n=4 and 10124 Å ($n=5 \rightarrow n=4$), 3203 Å ($n=5 \rightarrow n=3$), or 1055 Å ($n=5 \rightarrow n=2$) for n=5. The lines 4686 Å and 3203 Å

on the one hand and the lines 1215 Å and 1085 Å on the other hand form reasonable pairs, asking for similar equipment. In view of the problems connected with observation in the vacuum ultraviolet region, the pair 4686 Å and 3203 Å was selected despite of disturbing helium atom lines in the vicinity of 3203 Å.

The stable helium pressure was achieved by using a sealed glass system, thus avoiding the difficulty to control a continuous leak. Glass is guaranteed non-magnetic and, properly baked, has a very low outgassing rate. Moreover, a glass system can easily be filled with helium by diffusion through the heated walls[56]. This process at the same time purifies the helium (technical helium may be used), since all other gases including H_2 have much lower permeation rates[57].

Graded seals could be avoided by selecting glasses with expansion coefficients between 40 and $50 \cdot 10^{-7}/°C$ throughout. This allowed the ionization gauge head (Mullard, IOG 19) and the ultraviolet transmitting front window (Schott, glass 8337) to be joined directly to the body, and home made non-magnetic molybdenum feedthroughs to be used for the electrical connections to the electron gun.

The electron gun was mounted on three 1mm-molybdenum rods, insulated by sintered alumina tubing. Pieces of wider alumina tube were used for spacers. Most metallic parts were made from 0.2 mm tantalum sheet, which can be spotwelded easily and securely. This is important since no repairs can be made after the system is sealed. A commercial oxide coated cathode was used with 4 mm diameter emitting surface (M-O Valve Co Ltd, type DC 150 A). The body is ferromagnetic at room temperature, but heated to above the Curie point during operation. The present data show no

56 V.O. Altemose, J. Appl. Phys. 32, 1309-1316 (1961)
57 J.R. Young and N.R. Whetten, Rev. Sci. Instrum. 32, 453-454 (1961)

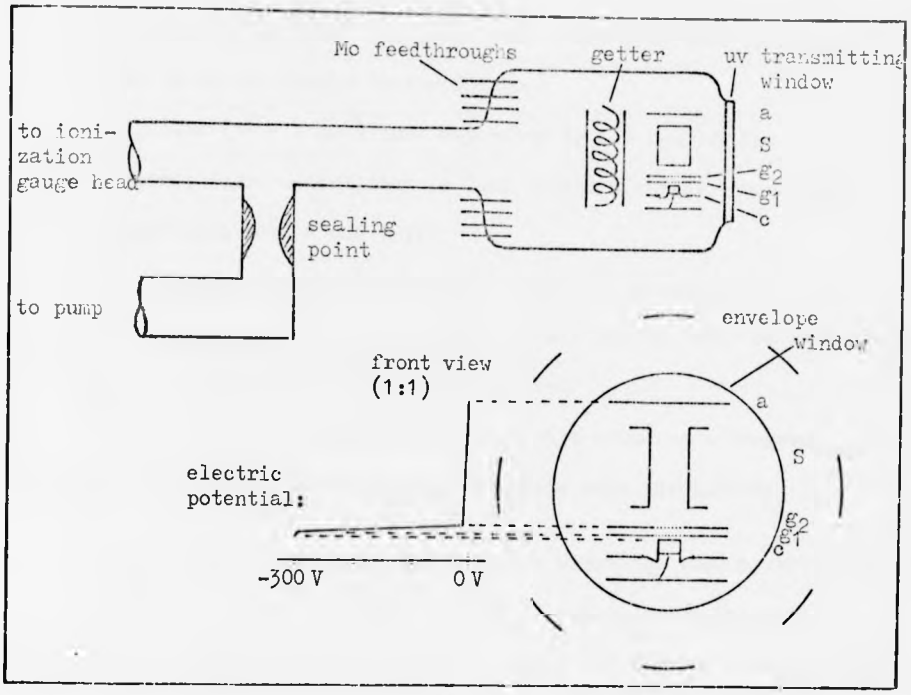

Fig. 9: Electron gun system. The upper part shows a side view in about half the original size, the front view in the lower part is drawn to scale. a: anode, S: Stark plates, g_2: grid 2 (accelerator), g_1: grid 1 (current control), c: cathode.
The usual voltages are indicated to the left of the front view.

significant effect of the magnetic field caused by the dc heating current of 400 mA. This was checked by reversing the current.

Two grids (M-O Valve Co Ltd, type DGL 4A) were mounted on tantalum apertures, g_1 to control the electron current, and g_2 to accelerate the electrons to the desired energy, normally about 300 eV. The voltage between cathode and grid 1 is controlled by an electronic regulation circuit sensing the anode current. This helps to stabilize the current in the observation region during variation of the electron energy or

of the magnetic field. The remaining current changes were -5% for a magnetic field varying from 1100 G to 11 000 G and less than 1% over the region used to detect single anticrossings.

The Stark plates (13×11 mm^2) were separated by 6.8 mm ± 5%. The reason for this fairly large uncertainty is that no Stark effect investigation was envisaged when tube 1 was built.

The anode, a simple tantalum plate, was earthed in order to keep the observation region near earth potential. Grid 2 was on -10 V so that slow electrons should drift towards the anode.

The getter consisted of a 0.23 mm titanium wire wound on 2 tungsten wires of similar size. The resulting composite wire was coiled.

To evacuate the glass system a small oilfree ultrahigh vacuum system was set up using a sorption pump (Mullard VAP 2) and an 8 l/s ion getter pump (Mullard VKP 8). Stainless steel is used, and a glass to metal seal provides the transition to the glass part to be sealed off. All tubing has 25 mm diameter to retain a usuable pumping speed of the order of 1 l/s. The glass part of the system was baked at 400 °C for several periods of a few hours in a temperature controlled furnace. Heating tapes were used for the metal parts. Pressures below $1 \cdot 10^{-8}$ Torr were reached. After activation of the cathode the system was sealed off together with the ionization gauge head. It was then exposed to 1 atm of helium and heated to 240 °C. After approximately 5 hours the desired ionization gauge pressure of $1.4 \cdot 10^{-3}$ Torr was reached, corresponding to $1.1 \cdot 10^{-2}$ Torr of helium[58].

58 Vacuum Generators Ltd, Technical Information: Pressure Measurement, 01. 454 (1971)

The pressure rise inside the tube is very slow. After 3.5 months an increase to $1.8 \cdot 10^{-3}$ Torr was registered. However, no deterioriation of the He-spectrum ($\rightarrow$5.1) could be detected even after 18 months. The getter has not been used yet.

4.3 Magnetic field and field measurement

An electromagnet with 25 cm pole face diameter (Bruker, B-E25B8) has been installed together with a 6 kW power supply (Bruker, 150/40 Si 6ng). The specified short term regulation is 10^{-6}. With an air gap of 6.5 cm a magnetic field of up to 13.6 kG can be generated. To allow optimum adaptation to different experiments the air gap is continuously variable to a maximum of 15 cm without and 7 cm with ring shims. The ring shims, properly adjusted to the working gap and field, greatly improve the field homogeneity below saturation ($\sim$10 kG). A motor driven potentiometer, incorporated into the power supply, allows to sweep the magnetic field.

The accurate measurement of the magnetic field is achieved by a nuclear magnetic resonance (nmr) system (AEG, nmr-cabinet). The nmr-frequency is registered with an 8 digit counter (Hewlett Packard, 5245 L). The counter gate may be controlled externally by the quartz of the nmr system to display the magnetic field directly in Gauss. More important, the nmr signal may be locked for automatic and continuous retuning of the oscillator frequency, so that the actual field value is displayed all the time during a reasonably slow sweep of the magnetic field. Calibration marks can be obtained at intervals of 1 or 10 G. Introducing an appropriate link to the power supply it is furthermore possible to regulate the magnetic field at a preset value of 6 decades.

The uncertainty of the automatic field reading depends on the sweep rate of the magnetic field since, by the time a field value is displayed on the counter, the actual field has already changed. With approximately 5 readings/s and a sweep rate of typically less then 0.5 G/s, this difference is less than 100 mG. This is in addition of the measuring uncertainty of ± 10 mG. The preset value of the gyromagnetic ratio of protons in water in this system was measured against the counter standard to 4.257620 (5) kHz/G, compared with the currently adopted value[41] of 4.257597 (13) kHz/G. The difference of about 6 ppm is negligible at the accuracy of the present data. A standard frequency receiver (Rohde und Schwartz, type XKD) has been used later to check the internal standard of the frequency counter against the standard frequency of 200 kHz, emitted from the Droitwich transmitter. The counter standard was fast by $1.2 \cdot 10^{-7}$, negligible in the present circumstances. This has been corrected, and checks are being made at intervals.

The field inhomogeneity over the interaction region was measured to be of the order of 10 ppm with negligible effect on the results taken. During the measurements however, the magnetic field had to be monitored at a distance of 4 cm from the interaction region. The field difference between the two positions (typically about 0.3 G) depends on the magnetic field strength. It was measured at the end of each session, and the final results were corrected accordingly.

4.4 Application of a radio frequency field

The application of a microwave field was considered necessary at least for the investigation of the Lamb shift in n=5 of He^+ since the only anticrossings between $5S_{1/2}$ and $5P_{1/2}$ occur at low magnetic field (βe at 490 G, βf at 1006 G), where previous experience[18,59] had shown considerable fluctuations of the light intensity with the magnetic field (→5.1.3). Much thought has been given to the problem of generating a suitable electric microwave field at the observation region. In view of the difficulty in obtaining microwave feedthroughs (in particular bakable ones), it was considered to apply the radio frequency from outside through the glass walls. The possibility was investigated of using an open structure resonator of the confocal Fabry-Perot type[60-62]. Such a device had been used successfully at 30 GHz by Narasimham and Strombotne[63] inside the vacuum chamber. Application at lower frequencies of 5-10 GHz seems feasible, but an experimental investigation would have to be carried out, especially regarding the influence of the glass walls.

59 H.-J. Beyer, Diplomarbeit, Universität Tübingen, 1967 (unpublished)
60 A.G. Fox and Tingye Li, The Bell System Technical Journal 40, 453-488 (1961)
61 G.D. Boyd and J.P. Gordon, The Bell System Technical Journal 40, 489-508 (1961)
62 H.K.V. Lotsch, Optik 30, 1-14, 181-201, 217-233, 563-576 (1969/70)
63 M.A. Narasimham and R.L. Strombotne, Phys. Rev. A 4, 14-32 (1971)

4.5 Light detection and signal recording

The electron excitation cross sections for the HeII-lines are only of the order of 10^{-20} cm^2, and it is of paramount importance to obtain a high detection sensitivity. The first problem is to isolate the respective lines. For the line 4686 Å this was achieved with a narrow-band interference filter[64]. However, it is difficult to produce such filters for the ultraviolet region, and no useful filter could be obtained for the line 3203 Å from n=5, which therefore had to be isolated by a monochromator (McPherson, model 218[65]). This instrument combines high light power with good dispersion, but its narrow entrance slit still resulted in a drastic reduction of the detected light intensity as compared to an interference filter.

When using the interference filter an enlarged image (2:1) of the interaction region was produced near the filter plane to reduce the divergence of the light beam on the filter side (the passband varies with the angle of incident light). An aperture in the image plane rejected light not originating from the region between the Stark plates. With the monochromator an image of approximately 1:1 was created in the plane of the entrance slit, which again selected light from between the Stark plates only.

A linear polarizer (Polacoat Inc, Pl 40) could be inserted into the light beam to select π or σ components of the lines.

The light was detected by a 13-stage photomultiplier (EMI, 9635 QA), selected for high sensitivity. It was screened with a Mu metal cylinder

64 Spectrum Systems, 5 cm diameter, centred at 4682.3 Å, halfwidth (FWHM) 7.4 Å. Transmission at centre 40%, transmission at the nearest other helium line (4713 Å) 0.01 %

65 f/5.3, 30 cm focal length crossed Czerny-Turner. The grating used is blazed at 3000 Å and ruled with 2400 gr/mm. Reciprocal linear dispersion 13.3 Å/mm

at cathode potential and operated at a distance of approximately 50 cm from the centre of the magnetic field with no apparent influence of the field on its performance.

The anode current of the photomultiplier was measured with a piccammeter (Keithley, model 417), which allows zero suppression so that small signal variations could be expanded. The output was applied to a x-t-recorder (Bryans, model 27000) through a variable RC-circuit. The event marker of the recorder was driven by the relay of the nmr-unit to provide calibration marks of the magnetic field simultaneously with the signal.

No modulation of the electric field has been attempted for two reasons: Firstly, the light intensity changes with the electric field even outside anticrossing regions, so that a modulation would not extract the anticrossing signal only. Secondly, the comparison of two voltages results in the loss of half the measuring time, thus reducing the signal to noise ratio.

The application of photon counting technique has been considered with the aim of improving the signal to noise ratio by superposition of several runs. However, this poses stringent requirements on timing, readout, and on the magnetic field sweep, which then should really be done in steps. This is very difficult with an electromagnet, especially when the same steps are to be reproduced over several runs. The line 4686 Å showed anapproximate counting rate of 10^6/s (electron current 300 μA at 300 eV), sufficient to analyse single runs in dc mode, and even the reduced intensity from n=5 will still allow such treatment.

5 MEASUREMENTS AND DATA ANALYSIS

5.1 Investigation of HeI- and HeII-lines

5.1.1 Complete spectra

Using the monochromator[65] the spectrum of tube 1 has been recorded between 2500 Å and 5050 Å in zero magnetic field at an electron energy of 250 eV. Some 60 lines could be ascribed to HeI- and HeII-transitions. 4 further weak lines, having the same excitation functions as HeI-lines and being symmetrically spaced on both sides of very strong atom lines, were identified as ghosts. Only two other very weak lines could not be identified, showing that tube 1 produces a very pure helium-spectrum. The recording was repeated 18 months later, when no deterioration could be detected.

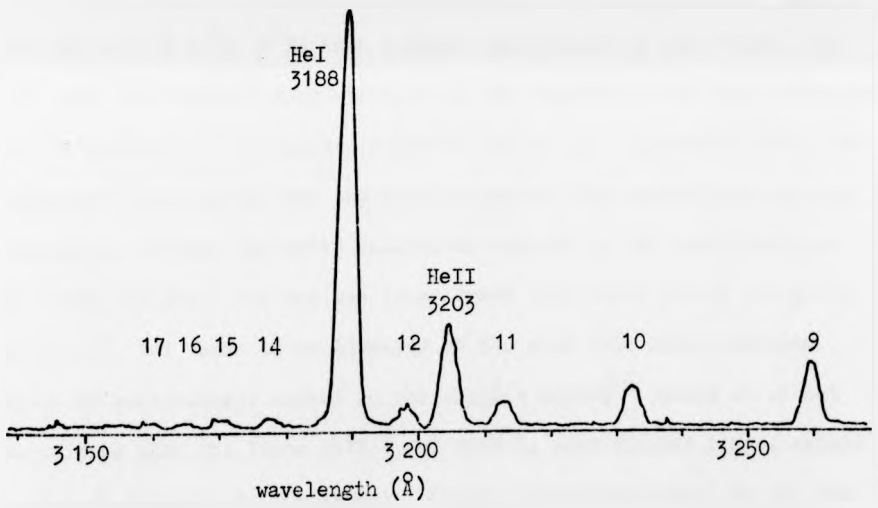

Fig. 10: Helium lines near 3200 Å, excited in zero magnetic field with 250 eV electrons in tube 1. Monochromator as in footnote 65 with slits 0.2 x 10 mm^2. Apart from the lines HeI-3188 Å ($4^3P \rightarrow 2^3S$) and HeII-3203 Å ($n=5 \rightarrow n=3$) there are several members of the $n^1P \rightarrow 2^1S$ series, n being denoted above the respective lines.

5.1.2 Spectrum near the line HeII-3203 Å

In contrast to the region near the line HeII-4686 Å, where only one disturbing atom line at 4713 Å has to be considered, there are many atom lines in the close vicinity of the ion line 3203 Å (n=5→n=3). This is illustrated in Fig. 10, which shows the relevant section of the spectrum recorded as described in 5.1.1.

The conditions become even less favourable with application of a magnetic field (→ 5.1.3), and it is obvious that a fairly good monochromator is required to single out the line 3203 Å.

5.1.3 Line intensities in magnetic field

All line intensities increase in the magnetic field, however not in the same proportion. This is obvious from Fig. 11: The lines HeII-4686 Å and HeI-4713 Å ($4^3S \rightarrow 2^3P$) have similar intensities in zero field, but the atom line becomes much stronger in the magnetic field. This behaviour can be explained by secondary electrons which, in a magnetic field, are prevented from leaving the observation region. The probability of them undergoing further inelastic collisions depends on the cross sections at lower energies. For the ion lines these drop below 200 eV (→Fig. 12 in 5.1.4), but there is an increase of the atom line cross sections, which is particularly marked in the triplet system[66]. Hence it is not surprising that the lines 4713 Å and 3188 Å, both triplet lines, should become so dominant in the magnetic field, increasing from 1 to 10. The singlet lines near 3203 Å show a much lesser increase from 1 to 2, quite comparable with the increase of the ion line intensities from 1 to 1.5.

66 B.L. Moiseiwitsch and S.J. Smith, Revs. Mod. Phys. 40, 238-353 (1968)

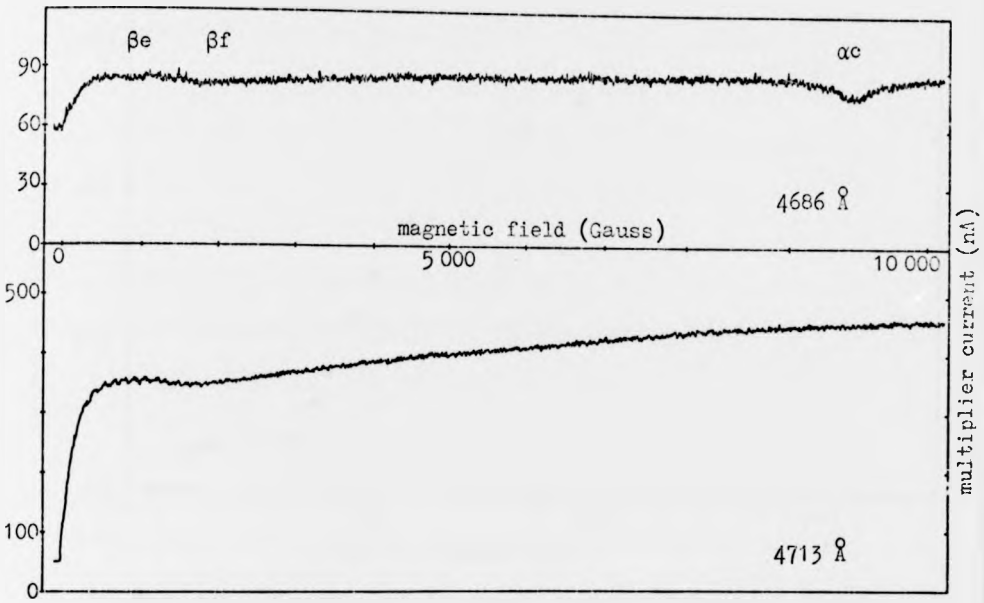

Fig. 11: Intensities of the lines HeII-4686 Å (top) and HeI-4713 Å (bottom) in dependence of the magnetic field. Tube 1, electron energy 250 eV. The anode current of 300 μA at zero magnetic field drops slowly to 280 μA at about 4500 G and then stays within 1%. Even without application of an external electric field internal fields in the observation region and motional fields are strong enough to induce S-P anticrossings in the ion line: αc at 9500 G and just a hint of βe and βf at 1000 G and 2000 G respectively.

5.1.4 Excitation function of the line HeII-4686 Å

Fig. 12 shows the excitation function of the ion line 4686 Å, taken through the interference filter[64] at a magnetic field of 2500 G. Above the threshold for atom lines in the visible region (approximately 23 eV) some background light is recorded. The ion line sets in above 76 eV (ionization + excitation to n=4) in agreement with previous work[37,67].

67 D. Haidt and H. Kleinpoppen, Z. Physik 196, 72-76 (1966)

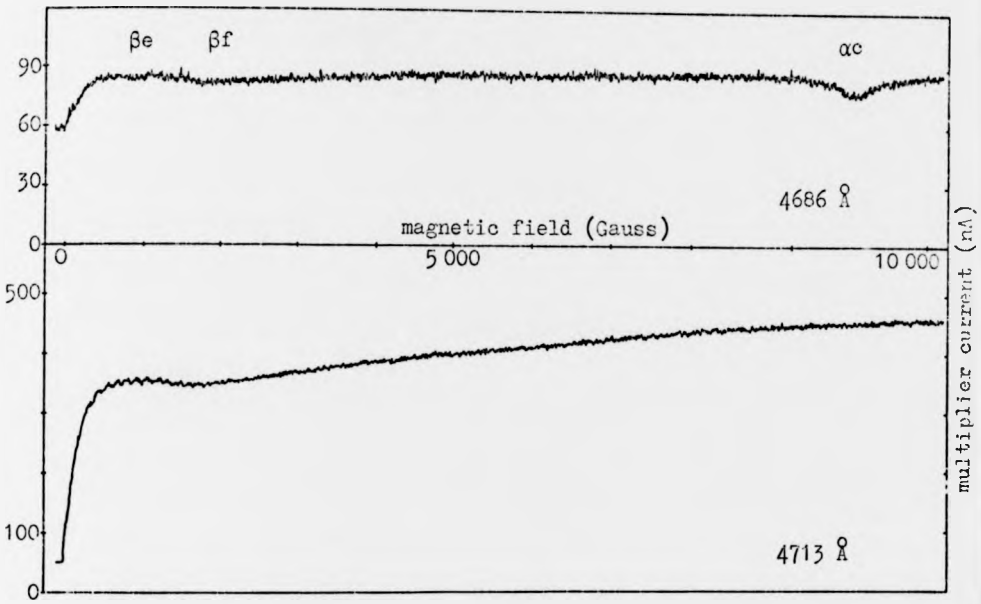

Fig. 11: Intensities of the lines HeII-4686 Å (top) and HeI-4713 Å (bottom) in dependence of the magnetic field. Tube 1, electron energy 250 eV. The anode current of 300 μA at zero magnetic field drops slowly to 280 μA at about 4500 G and then stays within 1%. Even without application of an external electric field internal fields in the observation region and motional fields are strong enough to induce S-P anticrossings in the ion line: αc at 9500 G and just a hint of βe and βf at 1000 G and 2000 G respectively.

5.1.4 Excitation function of the line HeII-4686 Å

Fig. 12 shows the excitation function of the ion line 4686 Å, taken through the interference filter[64] at a magnetic field of 2500 G. Above the threshold for atom lines in the visible region (approximately 23 eV) some background light is recorded. The ion line sets in above 76 eV (ionization + excitation to n=4) in agreement with previous work[37,67].

67 D. Haidt and H. Kleinpoppen, Z. Physik 196, 72-76 (1966)

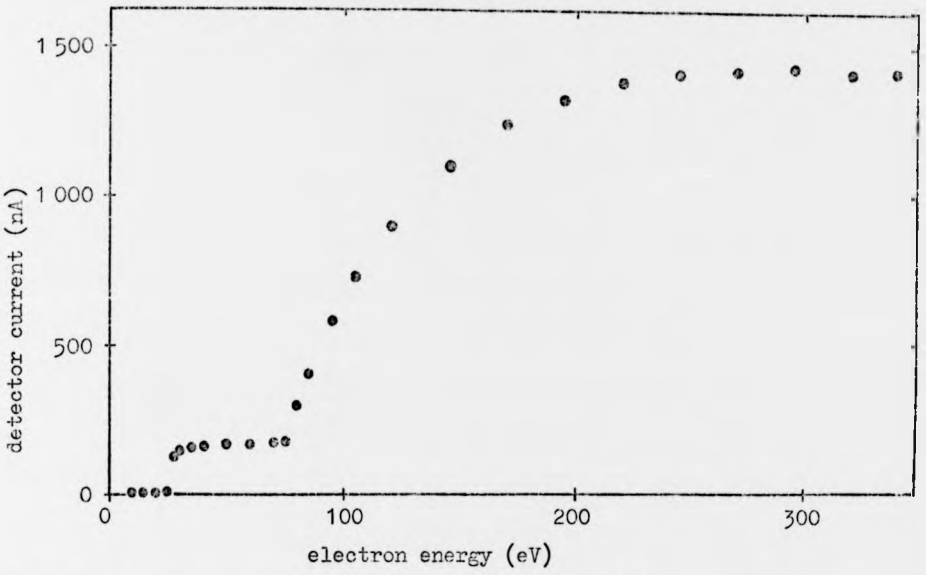

Fig. 12: Excitation function of the line HeII-4686 Å, recorded through the interference filter[64] at a magnetic field of 2500 G. Tube 1, grid 2 and Stark plates are connected and determine the electron energy. The anode potential is 10 V higher. Electron current 300 μA. Some atom line background is visible below the ion line threshold of 76 eV.

Compared with these investigations the peak of the excitation function is broadened and shifted to higher energies, obviously an influence of the magnetic field. The atomic background light is not so much ascribed to the line 4713 Å only, but to the whole range of atom lines, some of which are about hundred times as strong as the ion line (even without the magnetic field). This background is estimated to be fairly independent of the energy. At the working energy of about 300 eV it therefore represents approximately 12% of the total light and should not disturb the anticrossing investigation.

A slight polarization of the line 4686 Å was noticed parallel to the electron beam: P = 5.4% at 290 eV and 5400 G, not considering apparatus effects, which however should not be very marked with an interference filter. This agrees with previous results in zero magnetic field[67].

5.2 General investigation of anticrossings in n=4

All anticrossing signals detected in n=4 during the present investigation are collected in Table 3. It was considered difficult to improve the

S-F			S-D			S-P		
αN'	αG'	βH'	αJ	αE	βF	βe	βf	αc
5400	6700	7400	5800	8100	9800	1000	2000	9500

Table 3: Anticrossing signals observed in n=4 of He^+ and their approximate position in G. Lamb's notation of the sublevels is used (→Appendix 2).

measurement by Jacobs et al.[11] of the S-P intervals. Thus attention was given mainly to the S-D and S-F signals. From these βF overlaps with αc, and no use was made of this anticrossing although a set of curves, taken at various electric fields, indicated that a separation of the two signals might be possible since βF is much narrower than αc and requires 50.3 V/cm for 50% saturation compared with 6.9 V/cm for αc.

The other 5 S-D and S-F signals were first investigated using unpolarized light as well as linearly polarized π- and σ-light in order to select the working conditions providing the best signal to noise ratio. The S-D signals present the additional problem of the dispersion admixture (→3.1.3). The results of this investigation are displayed in Table 4.

detection mode	S-F % intensity change at 147 V/cm			S-D	
	αN'	αG'	βH'	αJ	αE
unpolarized	<u>+6.9</u>	>0 (+7.3)*	>0 (+4.6)*	-	<u>A+D (1:1)</u>+
σ -light	+7.7	<u>+18.5</u>	<u>+11.0</u>	<u>A+D (3:2)</u>+	mainly D
π -light	+6.0	-3.9	-2.5	very weak	<u>mainly A (7:1)</u>

*estimated. A:absorption, D:dispersion, approximate ratio A/D in brackets.
+the ratio of absorption to dispersion amplitudes does not remain constant for the whole electric field range. Considerable variations were noticed below 65 V/cm for αE (unpolarized) and below 85 V/cm for αJ (σ-light).

Table 4: Anticrossing signals in n=4 of He^+ for different light polarizations. The conditions finally used are underlined. Note the negative signals for αG' and βH' in π-light (see text). Examples of recorded curves are shown in Figs. 13-17.

The negative signals αG' and βH' in π-light appear to contradict the statement in Chapter 2 of an expected intensity increase for S-F signals. That statement however was based on the assumption of using unpolarized light for the detection, and the unpolarized signals αG' and βH' are indeed positive. Yet the sublevel H' cannot decay with π-light nor can G' in a strong magnetic field (Paschen-Back region), a condition substantially met at 6.7 kG. Thus H' and G' are "invisible" in π-light and so is any increase of their population near the crossing point. Hence anticrossing signals αG' and βH', observed in π-light, result only from the population reduction of the respective S-sublevels, which radiate unpolarized.

5.3 Data taking

The anticrossing signals with their working conditions chosen according to Table 4 were recorded on a chart recorder together with calibration marks of the magnetic field, as described in 4.5. Actual recorder traces are reproduced in Figs. 13-17. In Fig. 13 several recordings of the anticrossing βH', taken at different electric fields, have been superposed. This shows the typical features of the anticrossing signals under

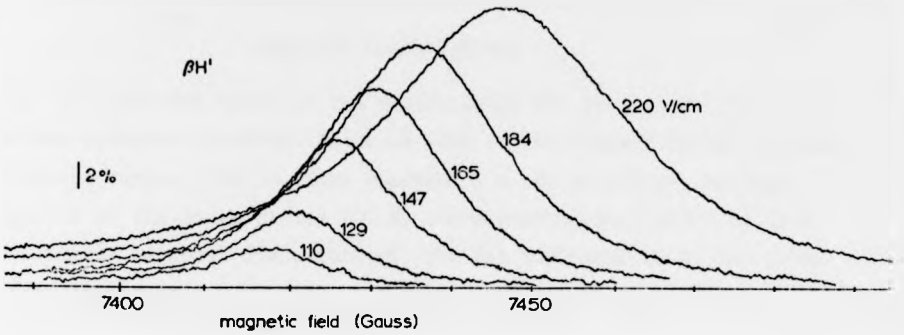

Fig. 13: Superposition of several recordings of the anticrossing βH' in n=4 of He^+, taken at different electric fields. This shows clearly the influence of the electric field on amplitude, width and position of the signal. Helium pressure 10 mTorr. Anode at +300 V with respect to the cathode, electron current 300 μA. Time constant 3 s. G-light. The bar indicates approximately 2% of the total light intensity.

investigation: The electric field is required to induce a signal, which is very weak at low field strength. With increasing electric field the amplitude rises until saturation occurs, and the signal becomes broadened and shifted.

A continuous sweep of the magnetic field is used, and the effect of the time constant of the detecting circuit on the signal has to be considered carefully. A large time constant, in providing a good signal to noise ratio, requires a low sweep rate of the magnetic field to avoid undue distortion

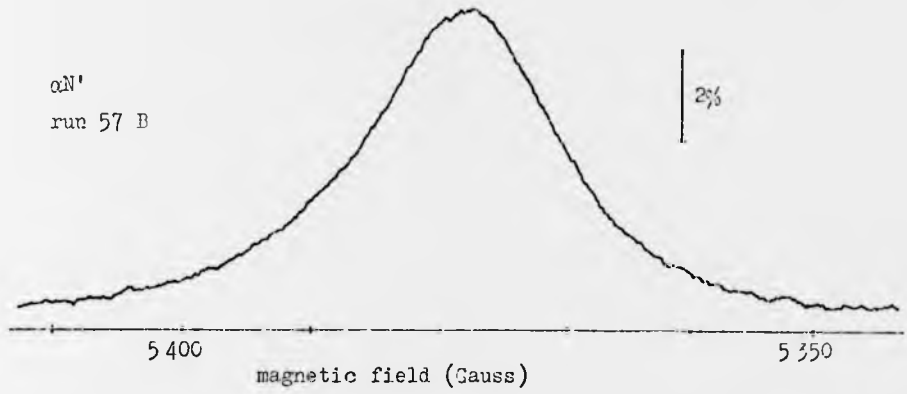

Fig. 14: Recorder trace of the anticrossing αN' in n=4 of He^+. Helium pressure 10 mTorr. Anode at +300 V with respect to the cathode, electron current 500 μA. Time constant 3 s. No polarizer. Voltage applied to the Stark plates 100 V, corresponding to (147 ± 7.5) V/cm. The signal is about 65% saturated. The bar indicates 2% of the total light intensity.

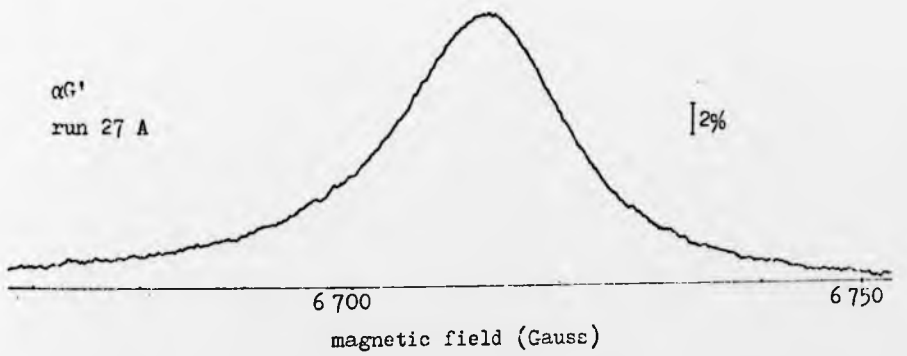

Fig. 15: Recorder trace of the anticrossing αG' in n=4 of He^+ using σ-light. Helium pressure 10 mTorr. Anode at +300 V with respect to the cathode, electron current 300 μA. Time constant 3 s. Voltage applied to the Stark plates 100 V, corresponding to (147 ± 7.5) V/cm. The signal is about 70% saturated. The bar indicates 2% of the total light intensity.

of the signals. On the other hand long term drifts influence the signals if too long measuring times are used. Expressing the sweep rate in terms of linewidths (FWHM) per time constant[68] a sweep rate of less than 0.1 was aimed at, resulting in some shift of the signal centre but in little actual distortion of the line shape. Most measurements were done at a sweep rate between 0.05 and 0.1 with a corresponding shift of the signal centres by $\lesssim$ 5% of the halfwidth. The recording time of one anticrossing curve was of the order of 5 minutes.

To eliminate this signal shift all signals were measured in pairs, sweeping the magnetic field upwards and downwards. The mean values of the parameters were adopted from each pair. This also eliminates other possible time lag effects of the magnetic field measurement and of the recorder as well as some long term drifts.

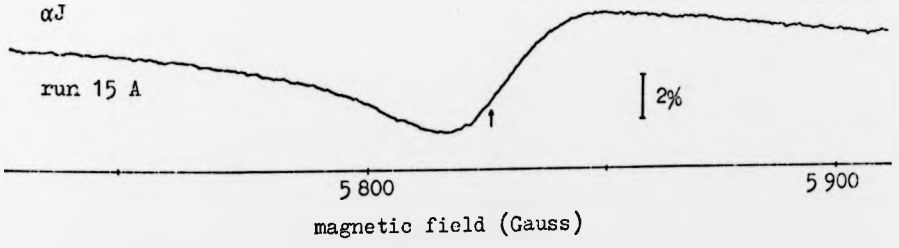

Fig. 16: Recorder trace of the anticrossing αJ in n=4 of He^+ using σ-light. Helium pressure 10 mTorr. Anode at +300 V with respect to the cathode, electron current 500 μA. Time constant 6 s. Voltage applied to the Stark plates 60 V, corresponding to (68 ± 4.5) V/cm. The signal is about 70% saturated. The bar indicates 2% of the total light intensity. The fitted centre is marked by an arrow.

68 R.C. Isler, J.O.S.A. 59, 727-733 (1969)

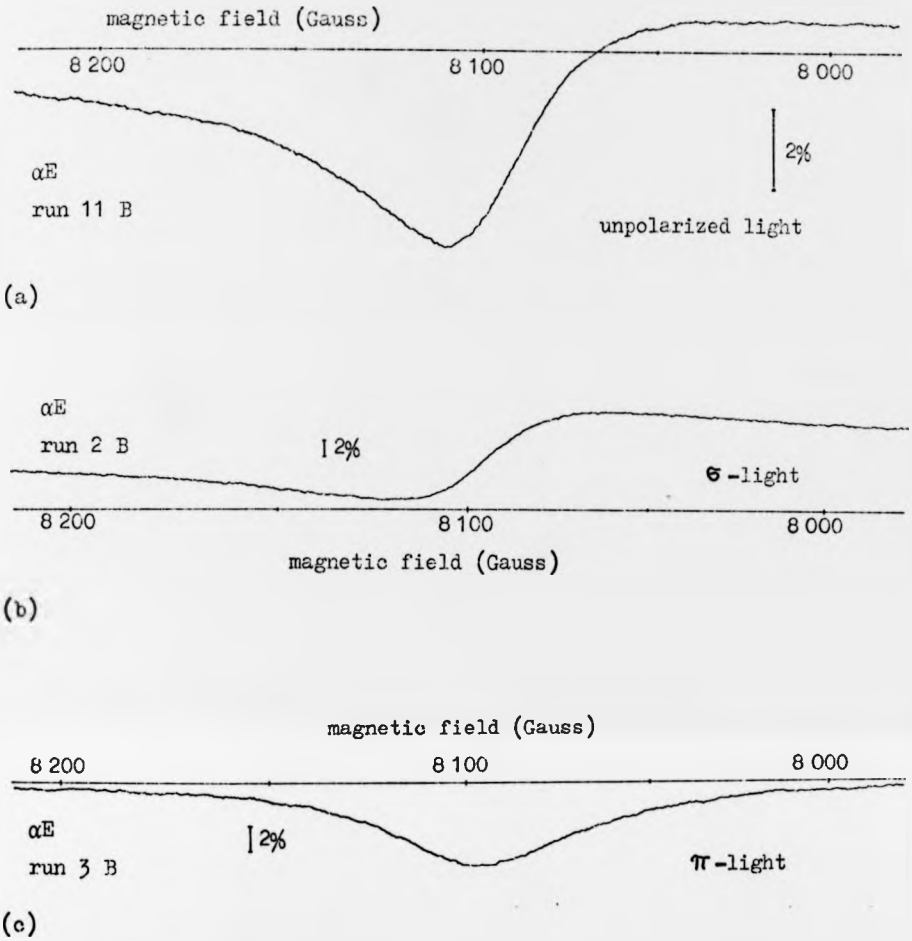

Fig. 17: Recorder traces of the anticrossing αE in n=4 of He^+.
(a) unpolarized light, (b) σ-light, (c) π-light. This illustrates how the dispersion admixture from the interference term (→3.1.3) modifies the absorption shaped signal at different states of polarization.
Helium pressure 10 mTorr. Anode at +300 V with respect to the cathode, electron current 300 μA. Time constant 6 s. Voltage applied to the Stark plates 40 V, corresponding to (59 ± 3) V/cm. The bars indicate 2% of the total light intensity.

5.4 Asymmetries of the signals

The recordings of the S-F anticrossings as in Figs. 13-15 show slight deviations from a pure absorption shape depending on the anticrossing and on the working conditions. Similar distortions would be expected for the S-D signals, were they not covered by the more complex structure of these signals. A whole variety of effects may contribute to these asymmetries.

(1) time constant of the detection circuit as discussed in 5.3

(2) slope of the background
(3) overlapping with other anticrossing signals of n=4 or n > 4 (cascading effects) not affecting the crossing sublevels directly
} additive

(4) change of the population difference with the magnetic field (quenching). Similar to (3), but affecting the crossing sublevels themselves
} dispersion admixture

(5) change of the interaction element V with the magnetic field

(6) inhomogeneity of the electric field (spatial variation of V over the interaction region). This results in a distorted line shape if the signal is appreciably shifted by the electric field.

(7) space charge- and motional electric fields. Similar to (6)

(8) deviation of the sublevel energies from the linear dependence on the magnetic field. In this case the replacement of $\Delta\nu$ by $(H - H_o)$ would not be correct.

The effects (1), (5), and (8) are considered to be of little impact in the present circumstances: No visible change of the distortion could be observed from sweep up to sweep down (1). The variation of V with the magnetic field (5) and the curving of the sublevels (8) is beyond the accuracy attempted at present.

5.4 Asymmetries of the signals

The recordings of the S-F anticrossings as in Figs. 13-15 show slight deviations from a pure absorption shape depending on the anticrossing and on the working conditions. Similar distortions would be expected for the S-D signals, were they not covered by the more complex structure of these signals. A whole variety of effects may contribute to these asymmetries.

(1) time constant of the detection circuit as discussed in 5.3

(2) slope of the background
(3) overlapping with other anticrossing signals of n=4 or n > 4 (cascading effects) not affecting the crossing sublevels directly
} additive

(4) change of the population difference with the magnetic field (quenching). Similar to (3), but affecting the crossing sublevels themselves
} dispersion admixture

(5) change of the interaction element V with the magnetic field

(6) inhomogeneity of the electric field (spatial variation of V over the interaction region). This results in a distorted line shape if the signal is appreciably shifted by the electric field.

(7) space charge- and motional electric fields. Similar to (6)

(8) deviation of the sublevel energies from the linear dependence on the magnetic field. In this case the replacement of $\Delta\nu$ by $(H - H_o)$ would not be correct.

The effects (1), (5), and (8) are considered to be of little impact in the present circumstances: No visible change of the distortion could be observed from sweep up to sweep down (1). The variation of V with the magnetic field (5) and the curving of the sublevels (8) is beyond the accuracy attempted at present.

The inhomogeneity of the electric field from the Stark plates (6) together with the space charge- and motional fields (7) cause the electric field to be distributed over a certain field range. Usually this range is of the order of ±10 V/cm, and for all present signals the shift corresponding to such fields is small compared with the signal width. Therefore the measured signals are wider than they would be in an ideally homogeneous field if their position is affected by the electric field. This has been observed on the anticrossings αN' and βH'.

The signal can then be looked at as a superposition of curves induced by a field distribution. Even with a symmetric distribution asymmetries of the signals can arise from the non-linearity of the Stark shift and from the field dependence of the amplitude. (Signals are usually observed below saturation so that the degree of saturation is larger on the high field side than it is on the low field side.) With the field range being only a small proportion of the actual field, these asymmetries remain small, and luckily the two effects are not important at the same time: The relative amplitude variation is largest at low electric field (low degree of saturation), where however the corresponding Stark shift range is still small (quadratic Stark effect). At higher electric field on the other hand there is much more broadening, but the amplitude variation is small.

Two observations support this view that asymmetries caused by field inhomogeneities are not the most important contributions to consider: Firstly, the anticrossing αG', hardly shifted at all by the electric field, shows very much the same amount of distortion as strongly shifted signals do. And secondly, the strongly shifted signal αN' shows rather different distortions when observed in π- or σ-light.

The actual field distribution is not too well known, and no attempt has been made to unfold the measured signals. However, an estimate of the influence has been made (→6.4.1 (3) and (4)), showing that the signal shift would hardly exceed ±0.5 G. This is incorporated in the error estimates in 6.4.1 and 6.5.1.

Thus there remain the points (2), (3), and (4). A slight change of the overall light intensity with time (2) was observed, particularly at the beginning of experimental sessions, when it was measured to -0.8% in 10 min. This became less after 1 or 2 hours, but was still present in general. With good accuracy this slope may be taken as linear with time, i. e. linear with the magnetic field.

Even more important influences are considered to result from overlapping with other anticrossings of n=4 and with cascading effects of anticrossings in $n > 4$ (3), (4). In view of the large number of sublevels with $n > 4$ such distortions are rather likely, and similar cascading effects have been experienced in radio frequency investigations of the fine structure of such levels by Jacobs et al.[11] and by Mader et al.[69], who investigated this in some detail. (In special cases it is even possible to use cascading signals for proper measurements, → 5.6.2.) At the strong coupling fields necessary for S-D and especially for S-F signals most of the disturbing (lower order) signals are well in saturation and thus very broad. On the other hand the signals under investigation are very narrow. Therefore it should be reasonably accurate to approximate most of the overlapping by effects linearly dependent on the magnetic field.

With this in mind the original absorption Lorentzian shape of the S-F signals was extended to include a linear slope of the base line and a

69 D.L. Mader, M. Leventhal, and W.E. Lamb, Jr., Phys. Rev. A 3, 1832-1848 (1971)

dispersion admixture of the same centre and width. The measured results were fitted to a curve of this form, making shure at the same time that all signals were treated in the same way. The inclusion of a dispersion part allows the function to be used for the analysis of the mixed S-D signals as well, where only rough estimates would be possible without fitting.

5.5 Lorentz fit

Following the discussion in 5.4 the observed signals are approximated by a 6 parameter Lorentzian curve:

$$y = \frac{A}{1 + (x-Z)^2/B^2}\left\{1 + C(x-Z)\right\} + D(x-Z) + E \qquad (15)$$

A: absorption amplitude — E: background at $x = Z$
Z: magnetic field at centre — D: slope of baseline
2B: full width at half maximum — C: dispersion parameter

Between 20 and 30 pairs of values x_i, y_i were read from each recorded curve and fitted so that

$$S = \sum_i \left\{y(x_i) - y_i\right\}^2 = \text{minimum} \qquad (16)$$

A single step least squares fit is not possible. Thus a variational method was employed[70], in which only one parameter is varied at a time, although in the present fitting A and E are coupled at one stage. Estimated values for Z, B, A, and E have to be entered together with their initial variations ΔZ, ΔB, ΔA, and ΔE. A least squares fit is used for the parameters C and D which are less easily estimated from the curves.

Procedure: For 3 values of a parameter P (P, $P + \Delta P$, $P - \Delta P$) the sums of the squared deviations (S_1, S_2, S_3 respectively) are calculated. A parabola

70 K.-J.A. Kollath, Diplomarbeit, Universität Marburg, 1966 (unpublished)

is fitted through the 3 points (P, S_1), $(P+\Delta P, S_2)$, and $(P-\Delta P, S_3)$ to provide at its centre an improved value of the parameter, P_1, with a reduced sum of the squared deviations, S. The original P is now replaced by P_1, and the next parameter is varied. At the end of one cycle through E, A, B, and Z the variation of the parameters is reduced and a new cycle started. Each call for the sum of the squared deviations includes a least squares fit for the parameters C and D.

Checks on the convergence are made after each cycle, and in case of slow but steady convergence several cycles are skipped and interpolated instead. The ordinary fitting procedure is then restarted with the new values. The fitting process continues until the parameter Z and the sum of the squared deviations in 3 adjacent cycles change by less than predefined amounts. Usually about 10 to 15 cycles are executed.

The difference between fitted curves and measured signals was generally found to be within the noise limits of the measurements, suggesting that the 6 parameter function is at least a better approximation than the undisturbed absorption curve would be. The adopted fitting procedure is further supported by the observation that a difference of about 0.8 G between signals $\alpha N'$ recorded in π- and σ-light disappeared.

As expected from the asymmetries of the signals, the fitted crossing centres S-F differ systematically from the direct estimates, though rarely by more than 1 G. There is usually a slight difference of the parameters C and D between the two sweep directions, indicating a small contribution from the time constant deformation.

All results reported in Chapter 6 have been processed in this way. The very time consuming preparation for the computer enforced a restriction of the amount of material analysed. To overcome this, an automatic read out facility is being set up. It is also hoped to improve the fitting programme to obtain better information on the uncertainties.

5.6 Signals from n=5

Very few fine structure measurements exist for n=5 of He^+. High resolution spectroscopic investigations were reported by Berry[71] and by Kessler and Roesler[72] on the lines 3203 Å (n=5→n=3) and 10124 Å (n=5→n=4) respectively. A value for the Lamb shift interval $5^2S_{1/2} - 5^2P_{1/2}$ was derived[72], but with an accuracy of only about ±15%.

Employing radio frequency transitions Baumann and Eibofner[73] recently investigated the fine structure interval $5^2S_{1/2} - 5^2P_{3/2}$ and from that indirectly deduced the Lamb shift to an accuracy of about ±1%. However, even with an electron current of 20 mA and a time constant of 10 s their signal to noise ratio is not very good and makes the analysis rather laborious.

Estimates of the excitation cross sections and of the branching ratios from n=5 showed that anticrossing signals similar to those of n=4 should be observable in the line 3203 Å, and a rough survey revealed that this is indeed the case. A brief account of such signals is given in 5.6.1.

An even more interesting way to investigate the fine structure of n=5 is provided by the detection of anticrossing signals occuring in n=5 through their cascading effects in the line 4686 Å (n=4→n=3). This is described in 5.6.2.

5.6.1 Anticrossing signals in n=5 using the line 3203 Å

The same arrangement as for the signals in n=4 (→Fig. 8 in 4.1) has been used with only the monochromator replacing the interference filter in order to select the line HeII-3203 Å. Sweeping the magnetic field over a wide range and using low time constant and no zero suppression in the

71 H.G. Berry, J.O.S.A. 61, 123 (1971)
72 E.G. Kessler, Jr. and F.L. Roesler, J.O.S.A. 62, 440-446 (1972)
73 M. Baumann and A. Eibofner, Phys. Lett. 43A, 105-106 (1973)

detection channel, several S-P and S-F anticrossings were detected as shown in Table 5. No special search has been made for the missing S-D and S-G signals, of which the former might be very weak and the latter too narrow to be observed in this survey. Anticrossing signals S-G should be negative because G does not contribute to the line 3203 Å, so that only the depopulation of 5S would be detected.

5S - 5P			5S - 5F		
βf	αc	βd	αN'	αG'	βH'
1000	4900	7400	2800	3500	3900

Table 5: anticrossing signals in n=5 observed through the line 3203 Å together with their approximate magnetic field position in G. Lamb's notation of the sublevels is used (→Appendix 2)

The signal to noise ratio is much smaller than for corresponding signals in n=4. This is caused in the first place by the necessity to use the monochromator to single out the line 3203 Å, but also by the smaller excitation cross sections of n=5 and by the less favourable branching ratios from n=5 to n=3. Nevertheless, single sweeps can be analysed, and a careful investigation of these signals in n=5 should allow to improve

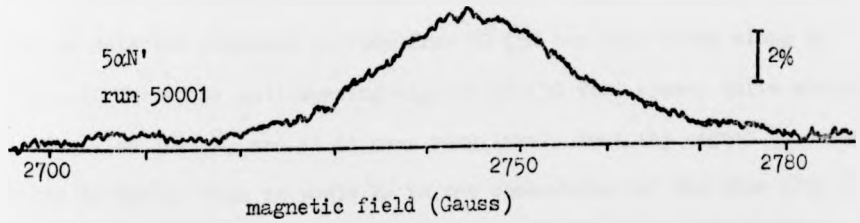

Fig. 18: Recorder trace of the anticrossing αN' in n=5 of He^+ detected in the line 3203 Å. Helium pressure 10 mTorr. Anode at +300 V with respect to the cathode, electron current 500 μA. Time constant 6 s. No polarizer. Voltage applied to the Stark plates 50 V, corresponding to (74 ± 4) V/cm. The bar indicates 2% of the total light intensity.

the experimental accuracy of the corresponding fine structure intervals. Fig. 18 shows a recorder trace of the anticrossing 5dN' at realistic working conditions. This has to be compared with the corresponding signal of n=4 in Fig. 14.

5.6.2 Cascading anticrossings from n=5

It has been pointed out in 5.4 that cascading effects from anticrossing signals occuring in n > 4 could distort the observed signals in n=4. These influences should be small though, since the excitation cross sections as well as the proportion of the high-n signals decaying through n=4 become smaller with increasing n. Nevertheless, Mader et al.[69] have been able to trace a cascading radio frequency signal from n=7 down in n=3, and for precision fine structure measurements it is necessary to consider these effects very carefully. In special circumstances it is even possible to employ such signals for the investigation of the corresponding higher n fine structure. This is the case with S-G anticrossings in n=5.

As in n=4, 5S is expected to be populated strongest. Thus anticrossings 5S - 5G result in less decay from 5S and more decay from 5G. Observing the line 4686 Å (n=4 → n=3), only about 1% of the change of population of 5S can be detected compared to 100% from 5G (5G can only decay along 4F, 3D,...). Therefore anticrossing signals 5S - 5G will appear quite strongly in the line 4686 Å, and it is even very likely that the signal to noise ratio is better than it would be in the observation of the line 3203 Å, direct from n=5. This is a result of the much greater detection efficiency of the line 4686 Å and of the very high difference of the branching ratios attainable in this way.

Using the same set-up as for the signals in n=4, a number of cascading anticrossings 5S-5G has been detected:

αQ"	αI"	αR"	βJ"
3000	2870	2400	3080

Table 6: Cascading anticrossings 5S-5G, detected in the line 4686 Å together with their approximate magnetic field position in G. For the notation of the sublevels see Appendix 2.

From these, αR" and αI" have been investigated in more detail to derive for the first time from direct measurements the fine structure intervals $5^2S_{1/2} - 5^2G_{7/2}$ and $5^2S_{1/2} - 5^2G_{9/2}$ respectively[74]. Fig. 19 shows a recorder trace of the anticrossing αR".

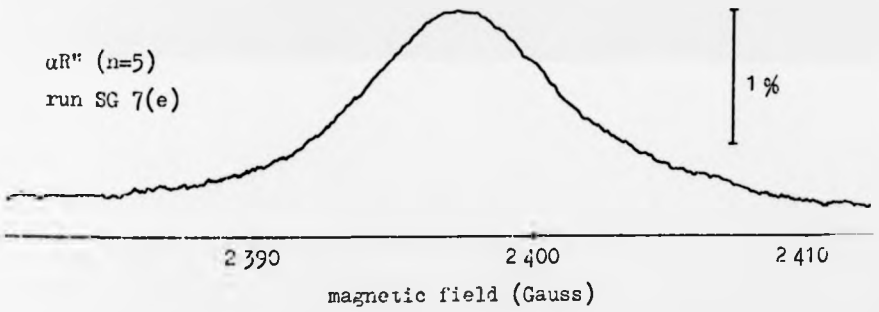

Fig. 19: Recorder trace of the cascading anticrossing αR" from n=5 of He^+ observed in the line 4686 Å (n=4 → n=3). Helium pressure 10 mTorr. Anode at +300 V with respect to the cathode, electron current 500 μA. Time constant 8 s. No polarizer. Voltage applied to the Stark plates 62.5 V, corresponding to (92 ± 5) V/cm. The bar indicates 1% of the total light intensity.

74 The detailed investigation has been carried out by J.M. Woolsey and is therefore not included in this report. For details see H.-J. Beyer, H. Kleinpoppen, and J.M. Woolsey, Phys. Rev. Letters 28, 263-265 (1972)

6 RESULTS

6.1 Saturation behaviour of the signals

Fig. 20 shows the experimental and theoretical results of the signal amplitude and the signal width in dependence of the electric field as discussed in 3.3. Again the anticrossing αG' is taken as example. The lines represent the theory, based on equations (2) and (3) in 3.1.2, for which the interaction element 2V has been calculated by the matrix diagonalization method ($2|V_{\alpha G'}|$ as function of the electric field is

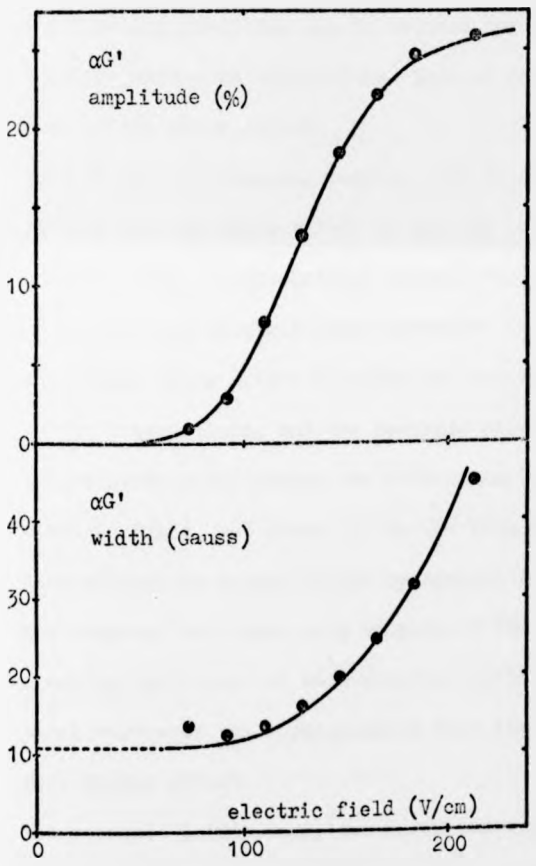

Fig. 20: Signal amplitude and signal width (FWHM) for the anticrossing αG' in n=4 of He^+ in dependence of the electric field. The points are measured. The theoretical lines are obtained using the interaction elements calculated by matrix diagonalization. The theoretical amplitudes are normalized to the experimental saturation value of 27.5%. Helium pressure 10 mTorr, electron current 300 μA at 300 eV.
The point size approximately represents the estimated experimental uncertainty, except for the lowest and highest field points, where the error could be larger (especially for the width). The lowest field point of the width seems to deviate from the theoretical value by more than the estimated uncertainty.

shown in Fig. 7 in 3.3). The amplitude is normalized to the estimated experimental saturation value of 27.5%. The agreement between theory and experiment is very satisfactory and verifies the assumptions made on the nature of these anticrossing signals.

6.2 Variation of the crossing positions with the electric field

Fig. 13 showed a very noticeable shift of the crossing position $\beta H'$ with the electric field. This is common to all observed higher order signals, and it is therefore necessary to extrapolate to zero electric field if the crossing positions are to be used for an accurate determination of the fine structure separations. This at the same time provides a measurement of the Stark effect.

Most of the experimental results used to derive the fine structure separations and the Stark effect in n=4 are collected in Figs. 21-25 and compared with the theoretical values. The data are drawn as a function of the squared electric field strength.

The simple Stark effect calculations according to 3.2.2 are represented by the dotted lines, and the accurate matrix diagonalization results according to 3.2.3 follow the full lines. As expected, both agree at low electric field, but above 150 to 200 V/cm (for n=4 of He^+) the matrix diagonalization method should be applied for accurate results.

The slope of the lines is a measure of the Stark effect. The theoretical crossing positions for zero electric field are determined by the theoretical values of the corresponding fine structure separations[7] and the pure Zeeman effect.

The measured points carry two error bars: The horizontal bars take account of the systematic uncertainty of the electric field strength, caused by

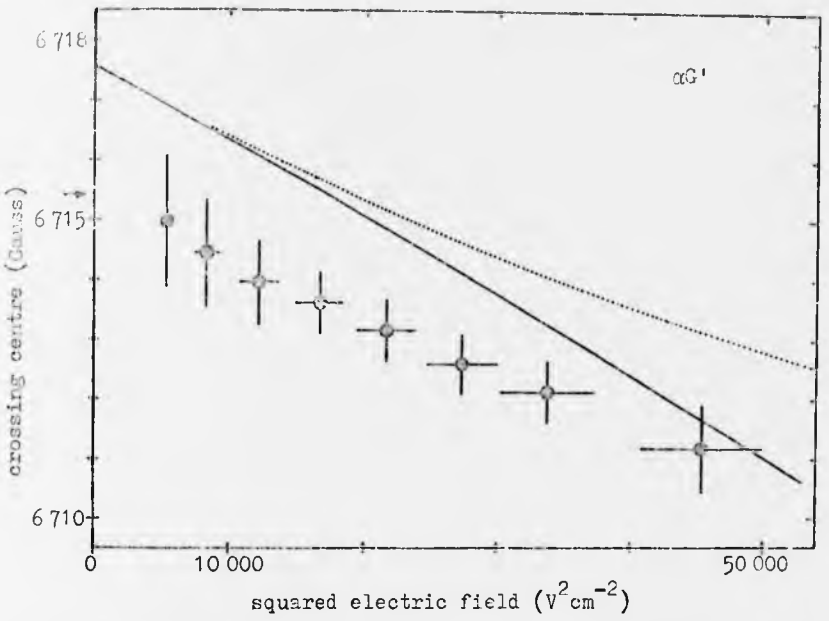

Fig. 21: Crossing position αG' in dependence of the squared electric field.

Figs. 21-25: Positions of the observed anticrossings in n=4 of He^+ as a function of the squared electric field. The lines in each graph represent the theoretical dependence, calculated in the simple approach according to 3.2.2 (dotted lines) and using the matrix diagonalization method according to 3.2.3 (full lines). Both start at the theoretical crossing point in zero electric field. Extrapolation of the measured points to zero electric field leads to the values marked by arrows, which determine the experimental fine structure intervals. The Stark effect is determined by the slope of the curves.

The horizontal error bars of the measured points are caused by a 10% uncertainty of the squared electric field. The vertical error bars represent the estimated uncertainty in finding the crossing centres with experimental conditions kept constant. A comprehensive discussion of the overall errors will be found in 6.4.1 and 6.5.1.

Helium pressure 10 mTorr, electron current 300 μA (except for Fig. 23: 500 μA), anode at +300 V with respect to the cathode.

Figs. 21-24 show an almost pure quadratic Stark effect.

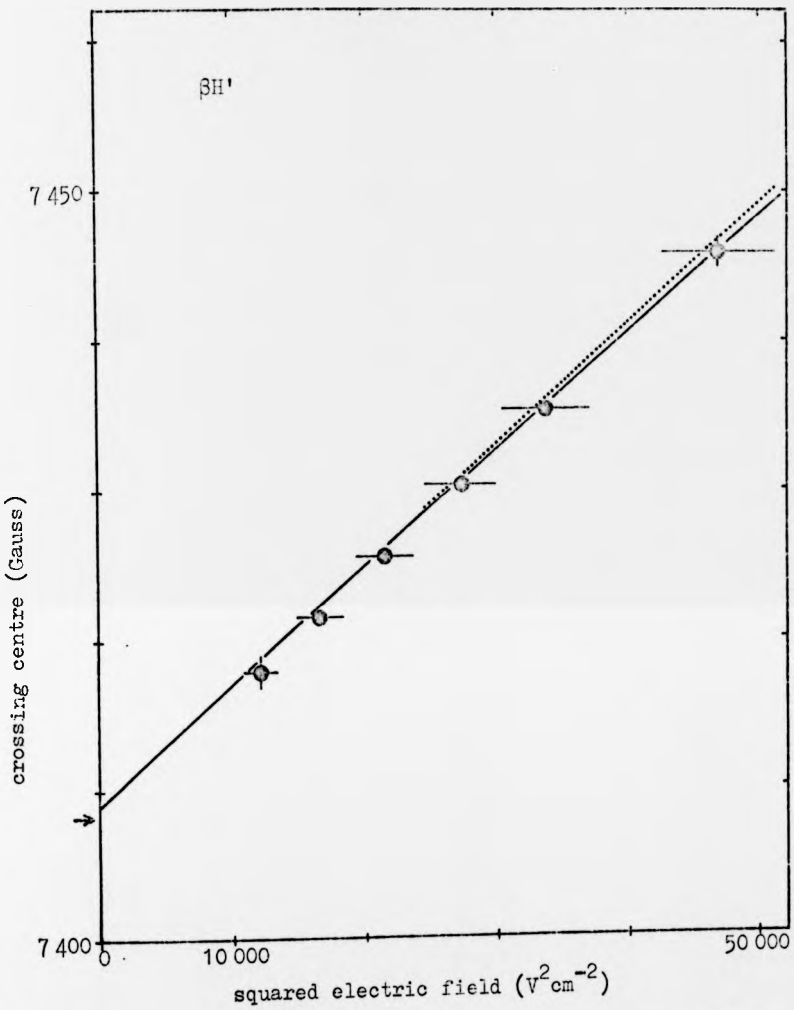

Fig. 22: Crossing position βH' in dependence of the squared electric field. → Fig. 21.

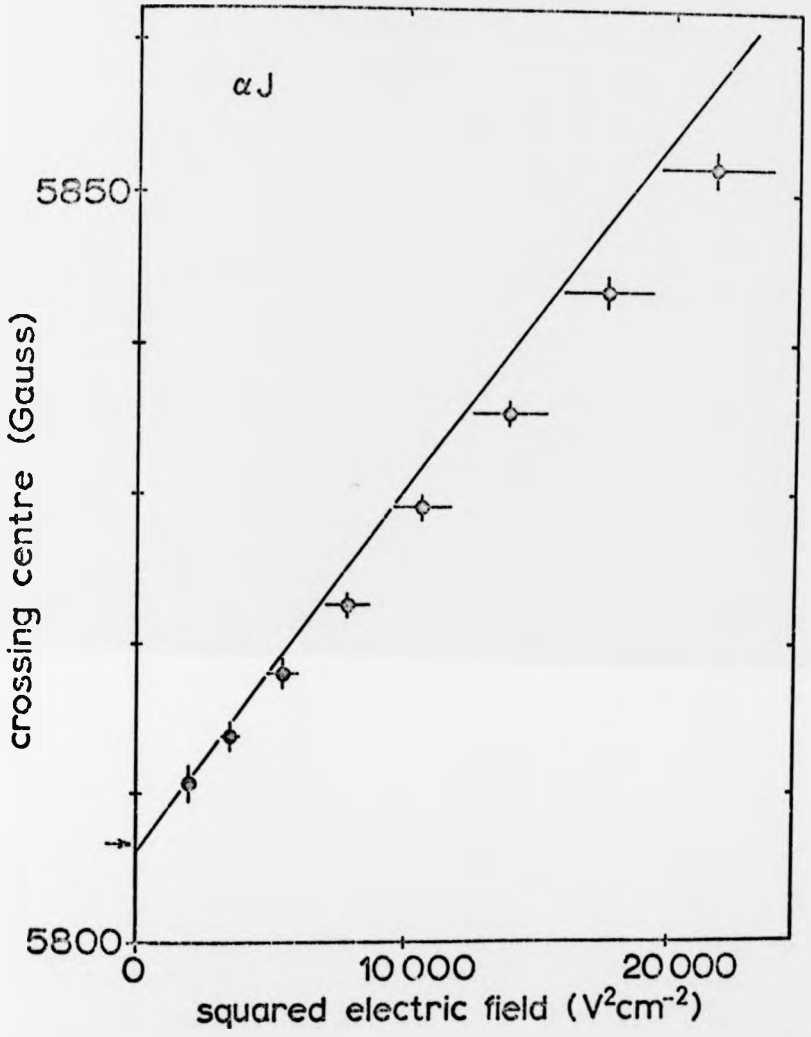

Fig. 23: Crossing position αJ in dependence of the squared electric field. → Fig. 21. Both Stark effect calculations coincide over this field range.

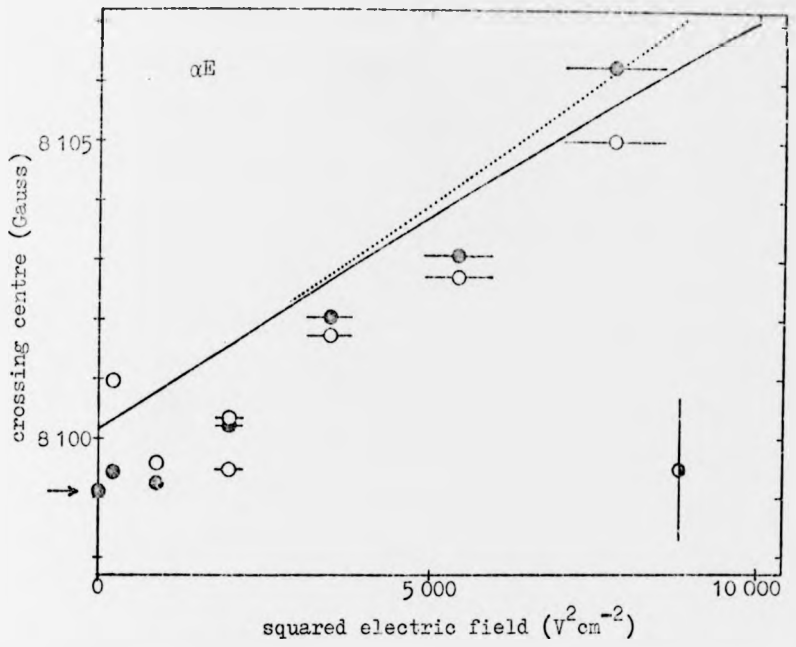

Fig. 24: Crossing position αE in dependence of the squared electric field. → Fig. 21.

the 5% uncertainty of the separation of the Stark plates. They are not very important for the fine structure results. The vertical error bars estimate the uncertainty in the determination of the crossing centres with experimental conditions kept constant. Further error contributions will be discussed together with the final numerical results in 6.4.1 and 6.5.1.

The theoretical Stark shifts of all anticrossings (apart from αN') are very nearly linear in a quadratic field scale: As expected, this field range is dominated by the quadratic Stark effect. Within the present experimental accuracy the measured results confirm the quadratic dependence. Unweighted least squares fits have been applied to the measured points to obtain the numerical zero electric field crossing positions (marked by arrows in Figs. 21-24) and the quadratic Stark constants.

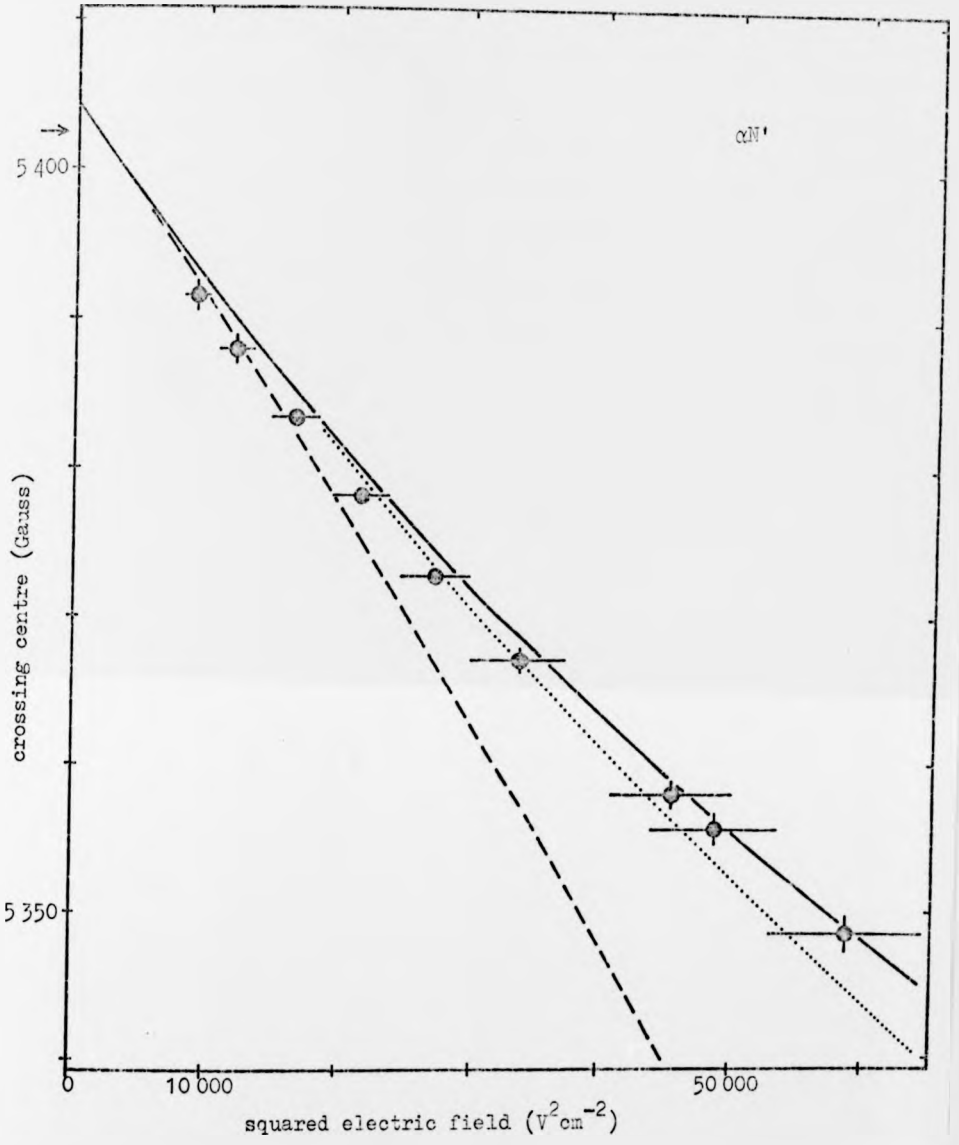

Fig. 25: Crossing position αN' in dependence of the squared electric field. → Fig. 21. Note the deviation from the pure quadratic Stark shift, which is represented by the dashed line. This start of the change from the quadratic to the linear Stark effect will be discussed further in 6.5.

6.3 Influence of electron current and helium pressure

The anticrossing signals are far less affected by changing the electron current or the helium pressure than by variation of the electric field. The observation region contains many electrons and positive helium ions, which are kept together by the strong magnetic field. Thus, a static electric field, perpendicular to the magnetic field, can penetrate this plasma without being appreciably screened. At higher electric fields however, the charges become partially separated in spite of the magnetic field, and this results in some screening of the applied electric field inside the observation region. The amount of this screening depends not only on the magnetic and electric fields, but also on the plasma density and hence on the electron current and on the helium pressure. It should grow with increasing current or pressure.

For the anticrossing signals this reduction of the effective electric field should result in a lower degree of saturation and less Stark shift. The slopes of the electric field dependences of the crossing positions should change more than the extrapolated zero field values. All anti-crossings should be affected in a similar way, somewhat modified by the absolute value of the magnetic field.

An investigation of the current effect has been made for the anticrossing signals αJ and $\alpha N'$. Fig. 26 shows the difference between the crossing positions measured for αJ at 300 μA and at 500 μA in dependence of the electric field. All points for 300 μA (full circles) lie above the points for 500 μA (open circles), indicating as expected a stronger Stark shift with decreasing current, although the difference is within the estimated uncertainty of single points. Least squares fits result in the full and the dashed line for 300 μA and 500 μA respectively. Their slopes differ

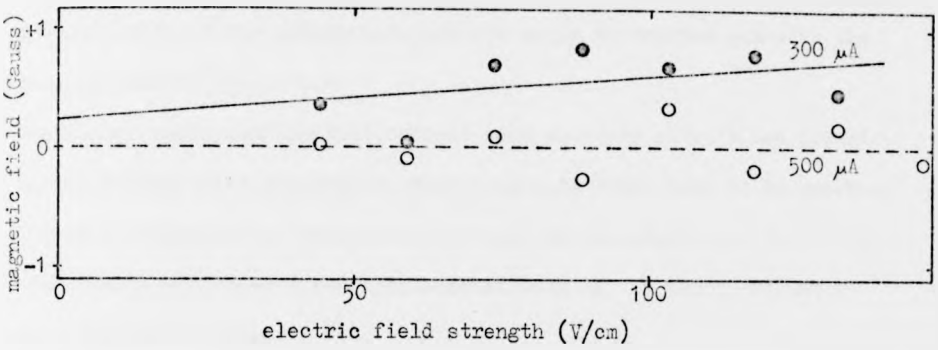

Fig. 26: Influence of the electron current on the measured crossing positions αJ in dependence of the applied electric field. The data are normalized to the dashed line, representing the least squares fit to the results at 500 μA (open circles). The continuous line is fitted to the results at 300 μA (full circles).

at the 80% confidence level, the extrapolated zero electric field values only at 60%.

The picture is similar for αN', where measurements have been made at 150, 300, and 500 μA. Again the Stark shift is reduced with increasing current for all points. The electric fields involved are larger here, but the Stark constant is smaller, and the current shift is slightly less than it was for αJ (0.25 to 0.5 G for 150 μA → 300 μA and again for 300 μA → 500 μA). Least squares fits are not possible in this case because of the curving of the electric field dependence as shown in Fig. 25, but no difference of the slopes is apparent here.

The screening model is further supported by the observation that the signal widths and the signal amplitudes also indicate a lower degree of saturation when the current is increased.

A variation of the helium pressure is expected to have a similar effect on the results as the current variation. The additional collision effects

are considered to be of minor importance at the pressure used. No actual investigation of the pressure dependence could be carried out with the present system[75].

The measurements confirm that current- and pressure effects are indeed small, though still detectable. Many more data would have to be analysed before a correction or extrapolation could be introduced. At this stage the effects have been taken into account only in the error estimates (→6.4.1 and 6.5.1).

6.4 Fine structure results

He^+, n=4 anticrossing positions (Gauss)						
anticrossing		present experiment		Eck & Huff	theory	statistical uncertainty
S-F	αN'	5402.4 ± 2.5		5350 ± 54	5404.45 ± 0.25	±0.3*
	αG'	6715.2 ± 2.5		6710 ± 67	6717.56 ± 0.32	±0.16 (14)
	βH'	7408.2 ± 2.5		7460 ± 75	7408.97 ± 0.32	±0.26 (11)
S-D	αJ 300 μA	5806.8 ± 2.0	5806.7 ± 2.0	~5900	5806.09 ± 0.35	±0.39 (7)
	αJ 500 μA	5806.6 ± 2.0				±0.28 (8)
	αE π	8099.4 ± 2.5	8099.1 ± 2.5	-	8100.15 ± 0.46	±1.1 (7)
	αE σ	8098.9 ± 2.5				±0.54 (7)

*estimated

Table 7: Crossing positions, extrapolated to zero electric field, in comparison with earlier measurements by Eck and Huff[18] and with the theoretical values. The last column shows the statistical uncertainty alone (90% confidence) together with the number of points used in the least squares fits. A detailed error discussion is given in 6.4.1.

75 The diffusion rate of helium through glass is proportional to the pressure difference between both sides of the wall. Thus the system cannot be emptied again by diffusion from 10^{-2} Torr. Only a further increase of the pressure would be feasible, but this was not desirable because of further measurements being planned with the same system.

The present results for the crossing positions, extrapolated to zero electric field, are collected in Table 7 and compared with earlier measurements by Eck and Huff[18] and with the theoretical positions. The values are derived from unweighted least squares fits to the data points measured at various electric fields as shown in Figs. 21-25. Only for αN' a graphical fit and extrapolation has been carried out. The overall errors shown are estimated for approximately 90% confidence limits. Their composition is discussed in 6.4.1.

Eck and Huff[18], using the same method, did not extrapolate their results to zero electric field. This explains the difference of the values for αN', βH', and αJ, although they all agree within the error limits. αG' is very little affected by the electric field and shows nearer agreement. The theoretical values are based on Erickson's[7] fine structure energies and the theory of the Zeeman effect (→3.2).

The fine structure separations corresponding to the results in Table 7 are obtained by calculating back to zero magnetic field, applying the Zeeman effect theory according to 3.2.2 or 3.2.3 (both give the same results). This is shown in Table 8. αG' and βH' both lead to the interval

He^+, n=4 fine structure separations (MHz)			
interval	anticrossing	present experiment	theory
$S_{1/2} - F_{5/2}$	αN'	27 435.7 ± 13.8	27 446.99 ± 1.36
$S_{1/2} - F_{7/2}$	αG'	31 094.8 ± 10.6	31 104.76 ± 1.36
		31 098.2 ± 10.5	
	βH'	31 101.5 ± 10.5	
$S_{1/2} - D_{3/2}$	αJ	20 145.3 ± 7.8	20 142.85 ± 1.36
$S_{1/2} - D_{5/2}$	αE	27 455.4 ± 7.4	27 458.60 ± 1.36

Table 8: Fine structure separations corresponding to the crossing positions in Table 7. The theoretical values are from Erickson[7].

$S_{1/2} - F_{7/2}$. The two values agree within the overall uncertainties given in Table 8, but they would not do so within the combined statistical uncertainties alone (1.8 MHz).

From the results in Table 8 the fine structure separations $F_{5/2} - F_{7/2}$ and $D_{3/2} - D_{5/2}$ and the Lamb shift interval $D_{5/2} - F_{5/2}$ can be deduced. Furthermore, the value of the interval $S_{1/2} - D_{3/2}$ may be combined with the latest value of (20 179.7 ± 1.2) MHz for the interval $S_{1/2} - P_{3/2}$, measured by Jacobs et al.[11], to derive an experimental value for the Lamb shift $P_{3/2} - D_{3/2}$. These results are shown in Table 9. They represent small differences of large intervals, and the relative uncertainties are therefore less favourable than in Table 8.

He^+, n=4 derived fine structure separations (MHz)		
interval	present experiment	theory
$F_{5/2} - F_{7/2}$	3 662.5 ± 23.0	3 657.78 ± 0.01
$D_{3/2} - D_{5/2}$	7 310.1 ± 14.3	7 315.75 ± 0.02
Lamb shift $P_{3/2} - D_{3/2}$	34.4 ± 9.0	37.19 ± 1.36
Lamb shift $D_{5/2} - F_{5/2}$	19.7 ± 20.0	11.61 ± 1.92

Table 9: Fine structure separations derived from the results in Table 8. The errors have been added linearly, deducting only component (2) d) of 6.4.1, which is identical for all signals. To obtain the Lamb shift interval $P_{3/2} - D_{3/2}$ the present result for $S_{1/2} - D_{3/2}$ is combined with the value of $S_{1/2} - P_{3/2}$ measured by Jacobs et al.[11]. The experimental uncertainties have been added in this case without consideration of the respective confidence levels.

All experimental results in Tables 7-9 agree with the theoretical values within the combined uncertainties. With the experimental uncertainties

representing approximately 90% confidence limits compared with 68% of the theoretical values, the experimental results in fact compare better with theory than it appears at first.

6.4.1 Error estimates for the fine structure separations

Theoretical values: All theoretical fine structure energies are calculated by Erickson[7], and their uncertainties are estimated at the 68% confidence level.

Experimental crossing positions:

(1) The statistical uncertainties of the extrapolated crossing positions are derived from the least squares fits to the data in dependence of the electric field (→6.2) and converted to the 90% confidence level. The values are shown in the last column of Table 7 together with the number of points used for each fit.

(2) Magnetic field

a) The absolute accuracy of the nmr-unit according to 4.3 is ~6 ppm ±3 ppm (from the gyromagnetic ratio) ± 10 mG. This results in less than 80 mG for all fields used and may be neglected.

b) The field difference between the probe position and the interaction region was of the order of 0.3 G and has been corrected. The uncertainty of this correction including the field inhomogeneity over the excitation region is estimated to ±0.1 G.

c) Sweep velocity. With about 5 readings/s there is a time lag between the actual field and the field displayed. Under the present sweep conditions this is less than 100 mG. The effect is mostly compensated by the recording of both sweep directions and can therefore be neglected.

d) Magnetic field generated by the cathode heating current (400 mA dc): Reversing the heating current had no observable influence on the signals. From this an upper limit of ±0.15 G is derived.

e) Reading the magnetic field values from the recorded curves introduces a statistical uncertainty, which is estimated to about ±0.4 G for S-F and ±0.7 G for S-D. However, with about 20 points used from each curve this mostly cancels out, and the remaining contribution to the statistical uncertainty of the signal centres should be reflected in the uncertainties of the least squares fits.

(3) Electric field

Several minor contributions cause the effective electric field to be slightly non-uniform in value and direction, and the mean field value might deviate from the value associated with the applied voltage on a geometrical basis:

A) Plasma screening. Direction opposite to the applied field (→6.3).

B) Field inhomogeneity introduced by the Stark plates (curving of the plates and edge effects).

C) Space charge fields. Random, mainly in the x,y-plane. A few V/cm[76].

D) Motional fields. Random, in the x,y-plane. In the present experiment about 7-11 V/cm depending on the magnetic field strength[76].

76 Estimates of the average internal electric fields (mainly resulting from C) and D)) can be derived from the widths of the three S-P anticrossing signals observed without external electric field using equation (3) from 3.1.2. Helium pressure 10 mTorr, electron current 300 μA at 250 to 300 V/cm.

αc (n=5)	4850 G	width: 310 G → el. field: 8.6 V/cm	(5.5 V/cm)
βd (n=5)	7400 G	width: 630 G → el. field: 11.0 V/cm	(8.4 V/cm)
αc (n=4)	9500 G	width: 380 G → el. field: 15.1 V/cm	(10.7 V/cm)

The values in brackets are the calculated average motional fields at a gas temperature of 400 K and the appropriate magnetic field. This shows that the motional fields represent the major part of the internal fields, an observation also made by Baumann and Eibofner (Ref. 73). It is expected that the contribution from space charge fields is reduced further when the external electric field is applied.

E) Misalignment of the electric field with respect to the magnetic field introduces a small field component in z-direction.

F) Electric fields from charged insulators. Despite the use of a glass system this effect is expected to be small since the excitation region is well screened by the conducting Stark plates.

Error contributions of electric field effects:

a) The ±5% systematic uncertainty of the separation of the Stark plates (→4.2) results in a ±10% uncertainty of the squared electric field strength. The relative deviation should however be independent of the electric field and of the anticrossings. Thus it results mainly in an uncertainty of the Stark constants and contributes little to the extrapolated crossing centres.

b) Uncertainties in the measurement of the Stark voltage and contact potentials are neglected.

c) The increase of the average electric field caused by the motional and space charge fields (randomly distributed in the x,y-plane) can be neglected since under the present conditions these fields represent only a small proportion of the external field. The resulting shifts of the signal centres have been estimated to $\lesssim$ 100 mG.

d) A possible misalignment of the electric field ($\vec{F}$ not exactly perpendicular to $\vec{H}$) would introduce a small field component in z-direction of certainly less than 10% of the applied electric field, with a corresponding reduction of the original field in x-direction by less than 0.5%. Owing to the quadratic field dependence of the Stark shift, and assuming similar Stark constants for x- and z-fields, both could affect the actual Stark shift by about 1%. This has negligible influence on the fine structure results.

e) Influence of plasma screening. → (5): Current and pressure shift.

f) Further influences of motional and space charge fields and of the field inhomogeneity → (4): Signal asymmetries.

(4) Signal asymmetries

The various possible causes for asymmetries have been listed and discussed in 5.4. It has been attempted to overcome the most important of them by the Lorentz fitting of the measured signals (→5.5). Apart from minor contributions, this disregards asymmetries caused by the motional and space charge fields and by the field inhomogeneity.

Their effect on the signals has been simulated by superposing 12 Lorentz signals with a range of centres and amplitudes as it might occur under experimental conditions as a result of the spread of the electric field strength. These superpositions were then fitted in the same way as real experimental signals in order to find the deviation of the fitted centres from the "true" centres.

This was compared with the position of the centre of gravity of only 3 Lorentz curves at fields $F - \Delta F$, F, and $F + \Delta F$, ΔF being the estimated maximum field deviation. Using the same field range, this produced larger shifts from the true centre than the 12 curves-superposition. It therefore gives a sensible upper limit and has been used to estimate the effect on the real data. Including motional fields only, but with the gas temperature generously set to 500 K to allow for other contributions, the error of the signal position did not exceed ±0.5 G.

No correction other than the Lorentz fit has been attempted, and even this hardly affects the signal positions by more than 1 G. Until the

assumptions made in 5.4 can be checked more closely, an overall systematic uncertainty of ±1.2 G has been included to cover the various kinds of asymmetries.

(5) Current and pressure shifts

The influence of the electron current and of the helium pressure on the observed signals has been discussed in 6.3, where also an investigation of the current shift is described. Further measurements are necessary before a correction can be made, but the present results provide a good basis to estimate the corresponding systematic uncertainty. ±1.0 G have been adopted for S-F, ±0.8 G for S-D.

The overall uncertainty of the extrapolated crossing positions is dominated by systematic errors, mainly resulting from (4) and (5). These contributions are added, and about 90% of the sum is combined with the statistical uncertainties to obtain the errors quoted in Table 7. The errors of the fine structure separations in Tables 8 and 9 follow directly from these values. The experimental errors are expected to represent at least 90% confidence limits.

6.5 Stark effect results

The experimental and theoretical Stark shifts of the various anticrossing signals are displayed in Figs. 21-25 in 6.2. Within the present accuracy and field range all signals apart from $\alpha N'$ can be considered to show a linear shift with the squared electric field, the pure quadratic Stark effect. The numerical quadratic Stark constants are derived from the least squares fits already introduced to find the extrapolated crossing positions. The results are shown in Table 10 and compared with the theoretical Stark constants based on the matrix diagonalization (→3.2.3).

anticrossing		theory	experiment		statistical uncertainty	field range
		$mG/(V/cm)^2$	$mG/(V/cm)^2$	$kHz/(V/cm)^2$	$mG/(V/cm)^2$	V/cm
S-F	$\alpha G'$	-0.131	-0.092 ± 0.022	-0.386 ± 0.092	±0.008 (14)	75-215
	$\beta H'$	+0.785	$+0.80 \pm 0.13$	$+3.34 \pm 0.54$	±0.01 (11)	110-215
S-D	αJ 300 μA	+2.36	$+2.13 \pm 0.36$	$+8.3 \pm 1.4$	±0.04 (7)	45-130
	αJ 500 μA	+2.34	$+2.09 \pm 0.34$	$+8.2 \pm 1.3$	±0.02 (6)	45-145
	αE π	+0.689	$+0.66 \pm 0.38$	$+1.9 \pm 1.1$	±0.28 (7)	15-90
	αE σ		$+0.89 \pm 0.27$	$+2.6 \pm 0.8$	±0.14 (7)	

Table 10: Experimental and theoretical Stark constants for the observed anticrossing signals in n=4 of He^+. The results are obtained in $mG/(V/cm)^2$, and these units are used for the comparison of theory and experiment. It is common to express quadratic Stark constants in frequency units/$(V/cm)^2$, but this is done for the experimental results only since the conversion factors are not strictly independent of the electric field.
The last column gives the electric field ranges used for the measurements and for the theoretical results. (The Stark constants vary slightly with the field range because of small deviations from the pure quadratic Stark effect.)
The quoted errors are estimated overall uncertainties (→6.5.1). The statistical uncertainties alone, representing 90% confidence limits, are shown in the second last column together with the number of points used for the least squares fits.

It is common to express the quadratic Stark constants in frequency units/$(V/cm)^2$. However, the conversion factors are not strictly constant with changing electric field owing to the large Stark constants under consideration. Therefore only the experimental results have been converted. This is also shown in Table 10.

The measured Stark constants range from 0.4 to 8 $kHz/(V/cm)^2$. These values are very large compared to Stark constants found in non-hydrogenic systems.

The reason becomes obvious when the energy difference between interacting levels is considered (the quadratic Stark shift is proportional to the inverse of this difference). The separation of interacting levels - usually of the order of 1 eV - is extremely small in the hydrogenic fine structure: In n=4 of He^+, 32 sublevels are spread over only 10^{-4} eV (30 GHz).

Considerable state mixing and deviation from the pure quadratic Stark effect occurs when the Stark shift becomes comparable to the level separation in zero electric field. At the various anticrossing points of this experiment the shift of the sublevels concerned ranges from 20 to 90 MHz at 100 V/cm and from 80 to 320 MHz at 200 V/cm, the shift of the anticrossing position being a differential effect between two such displacements. Displacements of this magnitude are certainly not always negligible compared with the level separations, and deviations from the pure quadratic Stark effect are therefore quite likely even at fields of 100 or 200 V/cm.

A close look at the theoretical field dependences of the crossing positions in Figs. 21-24 indeed reveals very slight deviations from the pure quadratic Stark effect. This may be disregarded at the present level of experimental accuracy. Nevertheless, the field ranges, for which the numerical results have been approximated by pure quadratic dependences, are given in the last column of Table 10.

The departure from the quadratic Stark shift becomes very obvious for the anticrossing signal $\alpha N'$ shown in Fig. 25. In this case the interacting sublevels N' and J are only 1550 MHz apart. The pure quadratic Stark shift of N', caused by J, would be 92 and 368 MHz for 100 and 200 V/cm respectively, thus being no longer small compared with the level separation even at such low fields. It has therefore been possible in this case

to observe the beginning of the transition from quadratic to linear Stark effect. In Fig. 25 of 6.2 both, theory and experiment clearly depart from the pure quadratic dependence represented by the dashed line.

In general the experimental results agree with theory well within the present error limits. Only for $\alpha G'$ do theory and experiment not overlap. However, the Stark shift here is only about 10% of the other results and therefore very sensitive to minor disturbing effects. Since all systematic uncertainties taken into account are fractional (→6.5.1), small absolute (but otherwise negligible) errors might represent a fairly large proportion of this result and so could account for the discrepancy. The most likely source is the overlapping with other signals (asymmetries).

6.5.1 Error estimates for the Stark constants

A detailed list of possible experimental uncertainties was given in 6.4.1 for the fine structure results. This list is followed again to estimate the uncertainties of the Stark constants.

(1) The statistical uncertainties of the slopes are derived from the least squares fits to the data in dependence of the electric field (→6.2) and converted to the 90% confidence level. The values are shown in the second last column of Table 10 together with the number of points used for each fit.

(2) Magnetic field

For the Stark effect only the shift, but not the absolute position of the anticrossings is important. Parts a), b), and d), being always the same, are therefore neglected. The contributions c) and e) are neglected for the same reasons as in 6.4.1.

(3) Electric field

a) The ±5% systematic uncertainty of the separation of the Stark plates is fully taken into account as ±10% uncertainty of the squared electric field strength and of the quadratic Stark constants.

Part of this uncertainty is attributed to curving and non-parallel adjustment of the Stark plates, resulting in a field inhomogeneity which has less severe effects on the signal position than a straight variation of the overall field strength. The 10% uncertainty of the Stark constants is therefore considered to cover most of the asymmetry effects as well, → (4).

b) and c) are neglected as in 6.4.1.

d) A misalignment of the electric field as estimated in 6.4.1 could affect the Stark constants by $^{+1}_{-2}$%.

(4) Asymmetries

From the asymmetry effects only the variation of the signal shift with the electric field has influence on the Stark constants. (3a) covers most of these effects, but an additional allowance of ±2% is made for the effects of the motional and space charge fields.

(5) Current and pressure effects

As explained in 6.3 these effects are expected to have a direct influence on the Stark shift. For αJ the Stark constant changed by +2% from 500 to 300 μA, though with a large statistical uncertainty. On this basis a systematic uncertainty of $^{+5}_{-3}$% has been included.

As in 6.4.1 about 90% of the linear sum of the systematic uncertainties is added to the statistical uncertainties to obtain the overall errors quoted in Table 10, which again should represent at least 90% confidence limits.

6.6 Final remarks

The fine structure results of this report are considerably more accurate than previous determinations[3,4,18], and for the first time in n=4 of He^+ it has been possible to measure the Lamb shift separations for $j > 1/2$. All experimental results agree with theory within the combined error limits, but the present values do not yet reach the theoretical accuracy.

Furthermore, the anticrossing method allowed to investigate the non-linear Stark effect of this fine structure system at low electric field. Considering the lack of such low field investigations in hydrogenic systems these measurements are very worthwile in spite of the restricted accuracy of the present results.

The value of these investigations would of course be enhanced by a reduction of the uncertainties. From the error composition it is clear that the main contributions result from systematic effects, and a considerable improvement of the accuracies would be achieved if these influences could be removed or at least thoroughly investigated and corrected. Apart from some modifications of the system (f.i. of the Stark plates) this requires the analysis of a large number of curves. Such a continuation of the experiment is planned, and as part of this programme an automatic read out facility is being set up at present.

Appendix 1

A general equation for steady state crossing signals has been derived by Wieder and Eck[43] and is reproduced below. Resonance fluorescence is assumed, but basically the results are also valid for electron excitation. Note that f_a, f_b is used in a different meaning from Chapter 3 of this work. Δ is equivalent to $\Delta\nu$.

"The steady-state anticrossing signal, expressed as a function of Δ and in terms of the properties of the eigenstates a and b (which do not vary appreciably over the region of the anticrossing), is

$$
\begin{aligned}
S = {} & (1/\gamma_a)\sum[\,|f_a|^2|g_a|^2\,] \quad (1) \\
& + (1/\gamma_b)\sum[\,|f_b|^2|g_b|^2\,] \quad (2) \\
& + (\gamma_a\gamma_b/\bar{\gamma}D)\sum[\,f_a f_b^* g_a g_b^* + f_a^* f_b g_a^* g_b\,] \quad (3) \\
& - (i\gamma_a\gamma_b\Delta/\bar{\gamma}^2 D)\sum[\,f_a f_b^* g_a g_b^* - f_a^* f_b g_a^* g_b\,] \quad (4) \\
& - (2|V|^2\gamma_a\gamma_b/\bar{\gamma}D)\sum[fg] \quad (5) \\
& + (2/\bar{\gamma}D)\sum[\,(V^* f_a f_b^* + V f_a^* f_b)(V g_a g_b^* + V^* g_a^* g_b)\,] \quad (6) \\
& + (\Delta\gamma_a\gamma_b/\bar{\gamma}^2 D)\sum[\,f(V g_a g_b^* + V^* g_a^* g_b) + g(V^* f_a f_b^* + V f_a^* f_b)\,] \quad (7) \\
& + (i\gamma_a\gamma_b/\bar{\gamma}D)\sum[\,f(V g_a g_b^* - V^* g_a^* g_b) + g(V^* f_a f_b^* - V f_a^* f_b)\,] \quad (8)\,,
\end{aligned}
\tag{1}
$$

where $D = \gamma_a\gamma_b + |2V|^2 + (\gamma_a\gamma_b/\bar{\gamma}^2)\Delta^2$ is the resonance denominator,

$$\bar{\gamma} = (1/2)(\gamma_a+\gamma_b),\quad f = (|f_a|^2/\gamma_a)-(|f_b|^2/\gamma_b),\quad g = (|g_a|^2/\gamma_a)-(|g_b|^2/\gamma_b)$$

and V is the matrix element of the static interaction which couples states a and b. The symbol f_a is an abbreviated notation for $f_{am} \equiv \langle a|\vec{f}\cdot\vec{r}|m\rangle$ the electric dipole matrix element for excitation to state a from state m. Similarly, $g_a \equiv g_{m'a} \equiv \langle m'|\vec{g}\cdot\vec{r}|a\rangle$ is the matrix element for spontaneous decay from state a to state m'. The starring of a quantity indicates its complex conjugate. The symbol $\sum$ before a set of brackets means that the quantity within the brackets is to be summed over all the relevant levels m, of the initial state, and m', of the final state in the resonance fluorescence process. All factors having to do with the intensity and spectral distribution of the resonance lamp, the spectral sensitivity of the detector, polarizations of incident and scattered light, experimental geometry, etc. are assumed to be contained in the matrix elements."

Appendix 2

	m= 9/2	7/2	5/2	3/2	1/2	-1/2	-3/2	-5/2	-7/2	-9/2
$G_{9/2}$	A" 4/+	B" 3/+	C" 2/+	D" 1/+	E" 0/+	F" -1/+	G" -2/+	H" -3/+	I" -4/+	J" -4/-
$G_{7/2}$		K" 4/-	L" 3/-	M" 2/-	N" 1/-	O" 0/-	P" -1/-	Q" -2/-	R" -3/-	
$F_{7/2}$		A' 3/+	B' 2/+	C' 1/+	D' 0/+	E' -1/+	F' -2/+	G' -3/+	H' -3/-	
$F_{5/2}$			I' 3/-	J' 2/-	K' 1/-	L' 0/-	M' -1/-	N' -2/-		
$D_{5/2}$			A 2/+	B 1/+	C 0/+	D -1/+	E -2/+	F -2/-		
$D_{3/2}$				G 2/-	H 1/-	I 0/-	J -1/-			
$P_{3/2}$				a 1/+	b 0/+	c -1/+	d -1/-			
$P_{1/2}$					e 1/-	f 0/-				
$S_{1/2}$					α 0/+	β 0/-				

Notation used for the magnetic sublevels of hydrogenic fine structure systems following Lamb. The m-values are preserved at all magnetic fields. At low field they correspond to m_j, at high field (Paschen-Back effect) they are made up from m_l and m_s as noted below each sublevel, + and - denoting $m_s = +1/2$ and $m_s = -1/2$ respectively.

J. Phys. B: Atom. Molec. Phys., 1971, Vol 4. L129–L132. Printed in Great Britain.

Fine structure measurement in He^+, $n = 4$ I. Intervals S–F†

H.–J. BEYER and H. KLEINPOPPEN
Department of Physics,
University of Stirling,
Stirling,
Scotland.

21*st October* 1971

Abstract. Electric field induced anticrossing signals are used to measure the fine structure splittings S–F of $n = 4$ in $(^4He)^+$. The crossing positions have been extrapolated to zero electric field. The present results are (27435·7 ±13·8) MHz for the interval $4^2S_{1/2}$–$4^2F_{5/2}$ and (31098·8 ±10·5) MHz for the interval $4^2S_{1/2}$–$4^2F_{7/2}$ in agreement with the theoretical values of (27446·99 ±1·36) MHz and (31104·78 ±1·36) MHz respectively. The interval $4^2F_{5/2}$–$4^2F_{7/2}$ is derived to (3663·1 ±24·3) MHz compared with (3657·78 ±0·01) MHz from the theory.

There have been many high resolution optical studies of the HeII λ 4686 Å ($n = 4 \rightarrow n = 3$) line complex to test the theory of the fine structure in hydrogenic systems, the most recent by Larson and Stanley (1967) and by Berry and Roesler (1970). Unfortunately the accuracy of the fine structure splittings derived from these investigations is limited by the Doppler width of the components, which greatly exceeds the natural width. Improved values for the S–P intervals were obtained however, when radio frequency methods were applied by Lea *et al.* (1966), Hatfield and Hughes (1967), Beyer and Kleinpoppen (1967), Jacobs *et al.* (1971).

The other intervals of $n = 4$ could not be investigated until Eck and Huff (1968, 1969) succeeded in observing crossing signals not only between S and P, but also between S and D and even between S and F. Using this method we have studied the S–F crossings in greater detail leading to the more accurate results reported here.

A static electric field is applied to He ions in the $n = 4$ states, produced by electron impact on ground state He atoms. The unresolved line complex λ 4686 Å ($n = 4 \rightarrow n = 3$) is observed. If the magnetic field is swept through the crossing points of certain sublevels, state mixing occurs resulting in changes of intensity and polarization of the line.

Wieder and Eck (1967) derived a comprehensive equation for level crossing signals. To couple states with different l values, a static electric field is required in addition to the magnetic field bringing the levels in question to the same energy. Such crossings are usually called anticrossings. A pure anticrossing, as represented by part 5 of equation (1) of Wieder and Eck (1967) does not require coherence in either the exciting or the decaying channel, but the two levels must have different populations and they must contribute to the observed line to a different extent. These conditions are present for the S-F anticrossings if a constant current of electrons is used to produce the excited ions. A signal of absorption Lorentzian shape is expected, when the magnetic field is varied through the crossing.

† First results were reported at the 3rd National Atomic and Molecular Physics Conference, 5–8 April 1971, York. The material was part of a paper presented at the 3rd EGAS Conference, 6–9 July 1971, Reading.

The experimental set up used to detect the anticrossing signals is shown in figure 1. It is similar to that of Eck and Huff (1969) and to that used before by the present authors (1967). A small glass system, containing an electron gun is evacuated, sealed off, and filled with about 10^{-2} Torr of helium by diffusion through the glass walls. Electrons of about 300 eV are used to produce the excited ions. The system is placed in a 10 inch electromagnet with the magnetic field parallel to the electron beam. A static electric field can be applied perpendicular to the magnetic field at two plates S.

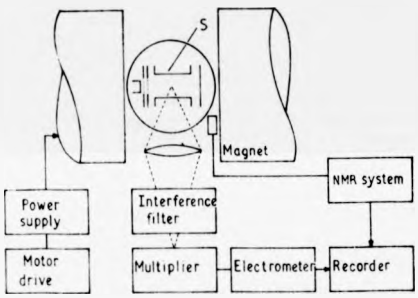

Figure 1. Experimental arrangement (see text).

The λ 4686 Å radiation from the region between these plates is detected at right angles to both electric and magnetic fields by a photomultiplier through a narrowband interference filter and a polarizer if appropriate. The signal is amplified with an electrometer and finally recorded with a chart recorder. The magnetic field is varied through the crossings with a motor drive and is continuously measured by a proton resonance system, which provides calibration marks on the recorder simultaneously with the observed signal. Each run consists of two curves, the magnetic field being varied upwards and downwards.

Figure 2 shows an actual recording of the anticrossing αN'†. Only a slight asymmetry is visible. This is believed to be caused mainly by overlapping with other anticrossings of $n = 4$ or higher states, which will be very much broadened at the comparatively high electric field strengths needed to couple S and F. Since the S–F anticrossings are very narrow it is hoped to approximate most of the overlapping by a linear slope of the background. Therefore a six parameter Lorentzian curve (including a linear change of the background and a dispersion admixture) was fitted to about 20 points read from each recorded curve. Depending on the actual crossing, the results for the centre obtained by this fit systematically differed from the direct reading by about 1 G. This method is supported by the observation that in the case of αN' small discrepancies between recordings taken in light polarized parallel or perpendicular to H were greatly reduced. Hence this fitting procedure was adopted throughout.

† We use Lamb's notation of the magnetic sublevels. It is shown with the results for the crossing points how these are connected with the conventional nomenclature in low field representation.

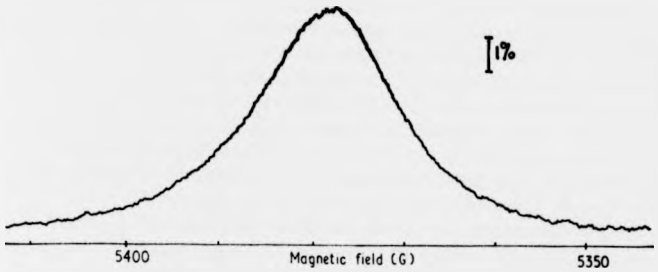

Figure 2. Recorder trace of the αN′ anticrossing in $n = 4$ of He^+. Helium pressure 10 mTorr. Anode at +300 V with respect to the cathode, electron current 500 μA. Time constant 3 s. No polarizer used. Voltage applied to the Stark plates 100 V, corresponding to (147 ± 7·5) V cm^{-1}. The signal is about 65% saturated.

Electric field strengths of the order of 130 V cm^{-1} are needed for 50% saturation of these anticrossing signals and fields of up to 230 V cm^{-1} are used for the present analysis. Such fields will of course shift the crossing centres due to Stark effect. Under the conditions used this shift is predominantly quadratic in the field strength. Displacements of more than 10 G for 50% saturation have been observed in two of the three anticrossings. Extrapolation of the crossing centres to zero electric field is therefore very important and has been carried out here. The electron current has generally been kept low (300 μA for the results below) to avoid excessive space charges in the interaction region. The variation of the current between 150 μA and 500 μA for the anticrossing αN′ produced only small shifts of about 1 G or less, apparently decreasing with decreasing electric field. No variation of the helium pressure has been carried out yet. Its effect is expected to be comparable in magnitude with the shift caused by the electron current.

The present values of three crossing points are shown below. The experimental results obtained by Eck and Huff (1968) are given in the braces.

(αN′)	$4^2S_{1/2}{}^{1/2} - 4^2F_{5/2}{}^{5/2}$	(5402·4 ± 2·5)G	{(5350 ± 53)G}
(αG′)	$4^2S_{1/2}{}^{1/2} - 4^2F_{7/2}{}^{5/2}$	(6715·5 ± 2·5)G	{(6710 ± 67)G}
(βH′)	$4^2S_{1/2}{}^{-1/2} - 4^2F_{7/2}{}^{-7/2}$	(7408·2 ± 2·5)G	{(7460 ± 74)G}

The Zeeman effect formulas given by Bethe and Salpeter (1957), including corrections for the nuclear motion and the anomalous magnetic moment of the electron, are used to obtain the fine structure intervals. The most recent theoretical values by Erickson (1971) are shown for comparison.

$4^2S_{1/2} - 4^2F_{5/2}$	(αN′)	(27435·7 ± 13·8) MHz		theory (27446·99 ± 1·36) MHz
$4^2S_{1/2} - 4^2F_{7/2}$	(αG′)	(31096·0 ± 10·6) MHz	(31098·8 ± 10·5) MHz	
	(βH′)	(31101·5 ± 10·5) MHz		theory (31104·78 ± 1·36) MHz

Combining these two intervals we obtain

$4^2F_{5/2} - 4^2F_{7/2}$	(3663·1 ± 24·3) MHz	theory (3657·78 ± 0·01) MHz

The uncertainties of the theoretical values are estimated by Erickson (1971) at the 68% confidence level. The experimental errors consist mainly of systematic uncertainties. We are confident that the actual values will be within the given limits.

The statistical uncertainty of the experimental results is computed for the $\beta H'$ anticrossing, which shows a quadratic shift with the electric field strength within our range. Applying a least squares fit we obtain the centre at zero electric field as shown above and its statistical error of $\pm 0{\cdot}26$ G (90% confidence level, 11 points used). The anticrossing $\alpha G'$ deviates slightly, and the anticrossing $\alpha N'$ clearly, from a quadratic dependence. The statistical uncertainty is estimated to be similar to $\beta H'$ in both cases, but some allowance would have to be made for the centre of $\alpha N'$ owing to the fact that the more complicated dependence might affect the accuracy of the extrapolation. From the systematic effects, only the most significant—the shift by the electric field—has been removed in this preliminary analysis. Other effects are being investigated further and have only been checked to be 'small', of the order of ± 1 G. Therefore the overall errors have been increased to $\pm 2{\cdot}5$ G as stated above.

We gratefully acknowledge the support given by the Science Research Council.

BERRY, H. G., and ROESLER, F. L., 1970, *Phys. Rev.* A, **1**, 1504–17.
BETHE, H. A., and SALPETER, E. E., 1957, *Quantum Mechanics of One- and Two-Electron Atoms*, (Berlin: Springer-Verlag).
BEYER, H.-J., and KLEINPOPPEN, H., 1967, *Z. Physik*, **206**, 177–83.
ECK, T. G., and HUFF, R. J., 1968, *Beam Foil Spectroscopy*, ed. S. Bashkin (New York: Gordon and Breach), pp 193–202.
—— 1969, *Phys. Rev. Lett.*, **22**, 319–21.
ERICKSON, G. W., 1971, private communication.
HATFIELD, L. L., and HUGHES, R. H., 1967, *Phys. Rev.*, **156**, 102–8.
JACOBS, R. R., LEA, K. R., and LAMB, W. E., Jr., 1971, *Phys. Rev.* A, **3**, 884–905.
LARSON, H. P., and STANLEY, R. W., 1967, *J. Opt. Soc. Am.*, **57**, 1439–49.
LEA, K. R., LEVENTHAL, M., and LAMB, W. E., Jr., 1966, *Phys. Rev. Lett.*, **16**, 163–5.
WIEDER, H., and ECK, T. G., 1967, *Phys. Rev.*, **153**, 103–12.

Fine structure measuren
II. Intervals S–D and L

H -J BEYER and
Department of Physic

MS received 25 Nove

Abstract. Electric fie
structure splittings S–
to zero electric field i
the interval $4^3S_{1/2}$–4^3
agreement with Eri
(27458·60 ± 1·36) MH
intervals to be (7310·
theory. Combining
provides a value for th
with the theoretical v

In a recent paper (Beyer and K
important references are given th
of the intervals 4S–4F in He^+ d
and experimental set up has bee

A static electric field is appli
electron impact on ground state
($n = 4 \rightarrow n = 3$) is observed. If
of certain sublevels, state mixing
tion of the emitted light.

For comparable saturation t
at the crossing points is only a
However, the signal strength is
the shorter lifetime of the D stat
the absorption lorentzian shape
is complicated by the fact that bo
level 3P. This gives rise to inte
to the pure anticrossing term, r
Eck (1967), the terms 7 and 8 o
in particular represents a dispe
signal and produces a mixed str

Such a structure can be seen
crossing αJ. The actual shape va
on the polarization of the light
strength applied to couple the
chosen in such a way that the

† Reported at the 3rd E.G.A.S. Conf

The method recently described

J. Phys. B: Atom. Molec. Phys. 5, L12–L15 (1972)

Fine structure measurement in He^+, $n = 4$. II. Intervals S–D and Lamb shift $P_{3/2}$–$D_{3/2}$†

H -J BEYER and H KLEINPOPPEN

Department of Physics University of Stirling, Stirling, Scotland

MS received 25 November 1971

Abstract. Electric field induced anticrossing signals are used to measure the fine structure splittings S–D of $n = 4$ in $(^4He)^+$. Extrapolation of the crossing position to zero electric field is carried out. The present results are (20145·3 ± 7·8) MHz for the interval $4^2S_{1/2}$–$4^2D_{3/2}$ and (27455·4 ± 7·4) MHz for the interval $4^2S_{1/2}$–$4^2D_{5/2}$ in agreement with Erickson's theoretical values of (20142·85 ± 1·36) MHz and (27458·60 ± 1·36) MHz respectively. The splitting $4^2D_{3/2}$–$4^2D_{5/2}$ is derived from these intervals to be (7310·1 ± 15·2) MHz compared with (7315·75 ± 0·02) MHz from the theory. Combining $4^2S_{1/2}$–$4^2D_{3/2}$ with $4^2S_{1/2}$–$4^2P_{3/2}$, measured by Jacobs *et al*, provides a value for the Lamb shift $4^2P_{3/2}$–$4^2D_{3/2}$ of Σ = (34·4 ± 9·0) MHz compared with the theoretical value of (37·19 ± 1·36) MHz.

In a recent paper (Beyer and Kleinpoppen 1971, a more general survey and other important references are given there), denoted as part I, we described a measurement of the intervals 4S–4F in He^+ derived from anticrossing signals. The same method and experimental set up has been used to study anticrossings 4S–4D.

A static electric field is applied to helium ions in the $n = 4$ states, produced by electron impact on ground state helium atoms. The unresolved line complex λ 4686 Å ($n = 4 \rightarrow n = 3$) is observed. If the magnetic field is swept through the crossing points of certain sublevels, state mixing occurs resulting in changes of intensity and polarization of the emitted light.

For comparable saturation the electric field strength required to couple S and D at the crossing points is only about half of that needed for the S–F anticrossings. However, the signal strength is reduced, and the signal width is increased because of the shorter lifetime of the D state compared to F. Furthermore—in comparison with the absorption lorentzian shape of the S–F signals—the shape of the S–D anticrossings is complicated by the fact that both levels involved (4S and 4D) can decay to a common level 3P. This gives rise to interference effects in the detection channel. In addition to the pure anticrossing term, represented by part 5 of equation (1) of Wieder and Eck (1967), the terms 7 and 8 of this equation might contribute to the signal. Part 7 in particular represents a dispersion lorentzian shape which adds to the absorption signal and produces a mixed structure.

Such a structure can be seen in figure 1, which shows a recorder trace of the anticrossing αJ. The actual shape varies from one anticrossing to another. It also depends on the polarization of the light used for the detection, and on the static electric field strength applied to couple the levels. If, however, the direction of polarization is chosen in such a way that the dipole selection rules forbid the decay to common

† Reported at the 3rd E.G.A.S. Conference, Reading, 6–9 July, 1971.

The method recently described by Beyer and ... ions in 5G decay to 4F and then only

sublevels of 3P, the interference effects should be removed and a pure absorption lorentzian shape should result. This has been observed for the anticrossing αE when π light was used for the detection. The ratio of dispersion to absorption amplitude

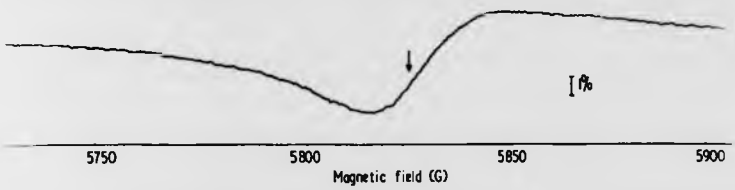

Figure 1. Recorder trace of the anticrossing αJ in $n = 4$ of He^+. Helium pressure 10 mTorr. Anode at +300 V with respect to the cathode, electron current 500 μA. Time constant 6 s, σ–polarization. Voltage applied to the Stark plates 60 V, corresponding to (88 ± 4·5) V/cm. The signal is about 70% saturated.

is reduced to about 1:10 from something like 1:1 when unpolarized light is used. The anticrossing αJ should show a similar effect. However, the signal disappears almost completely if π light is used.

It is not possible, in a straightforward way, to determine the crossing centres from the asymmetric signal recordings. Thus, in order to find the centres, a computer fit is made to the measured curves. This adjusts the ratio of absorption to dispersion signal and the other parameters. Only one additional parameter is needed to cope with the dispersion part, since the crossing centre and the width are the same for the different contributions. The six parameter program used to fit the S–F anticrossings in part I already had a dispersion admixture to deal with linear changes of the background. It could, therefore, be applied here without change. As in the case of the S–F anticrossings, linear variations of the background are fitted at the same time.

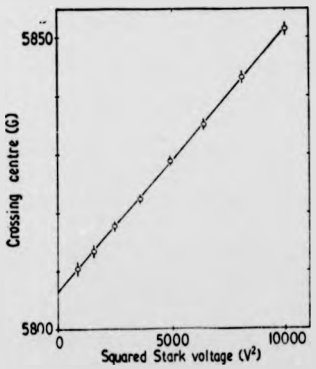

Figure 2. Position of the anticrossing αJ in dependence of the squared voltage applied to the Stark plates. The distance between the plates is 6·8 mm ± 5%. Helium pressure 10 mTorr. Electron current 500 μA, anode at +300 V with respect to the cathode. It should be noted that the electric field is needed to create the anticrossing signal. Hence the observed signal is very weak at low voltages and it is saturated and considerably broadened at the larger voltages of the diagram.

As in part I, extrapolation to zero electric field strength is necessary to obtain the proper crossing points. The shift of the crossing positions due to Stark effect is again predominantly quadratic with the field strength within the range used. The anticrossing αJ shows a particularly strong dependence, and this can be seen in figure 2. A straight line, corresponding to a purely quadratic dependence on the electric field, appears to fit the data best, and a least squares fit has been carried out to obtain the crossing point at zero field. There is a slight variation of the electric field dependence with the electron current: A reduction of the current from 500 μA to 300 μA resulted in a mean upward shift of the crossing points αJ by 0·5 G. There is, however, also a slight change in the slope, and the extrapolated value is only shifted by 0·2 G compared to statistical uncertainties for 90% confidence limits of $\pm 0{\cdot}28$ G (8 points) and $\pm 0{\cdot}39$ G (7 points) for 500 μA and 300 μA respectively.

A current of 300 μA has been used throughout for the anticrossing αE. The signal to noise ratio is not as good as for αJ and the points are somewhat more scattered. Following the discussion above on the signal shape two runs have been analysed in unpolarized and π light. The difference in the extrapolated value of 0·5 G is not significant since it is only a third of the sum of the statistical uncertainties (90%). These are $\pm 1{\cdot}1$ G (π light, 7 points) and $\pm 0{\cdot}56$ G (unpolarized light, 7 points).

For the two anticrossings observed we obtain the crossing points

$$(\alpha J)\ 4^2S_{1/2}^{1/2}\text{–}4^2D_{3/2}^{3/2} \qquad (5806{\cdot}7 \pm 2{\cdot}0)\text{G}$$

$$(\alpha E)4^2S_{1/2}^{1/2}\text{–}4^2D_{5/2}^{3/2} \qquad (8099{\cdot}1 \pm 2{\cdot}5)\text{G}$$

These anticrossing signals have been detected by Eck and Huff (1968, 1969), but only approximate values were derived. Using the theory of the Zeeman effect as in part I, we obtain the fine structure intervals at zero magnetic field.

$$4^2S_{1/2}\text{–}4^2D_{3/2} \qquad (20145{\cdot}3 \pm 7{\cdot}8)\ \text{MHz} \qquad \text{theory: } (20142{\cdot}85 \pm 1{\cdot}36)\ \text{MHz}$$

$$4^2S_{1/2}\text{–}4^2D_{5/2} \qquad (27455{\cdot}4 \pm 7{\cdot}4)\ \text{MHz} \qquad \text{theory: } (27458{\cdot}60 \pm 1{\cdot}36)\ \text{MHz}$$

Combining these two intervals we obtain

$$4^2D_{3/2}\text{–}4^2D_{5/2} \qquad (7310{\cdot}1 \pm 15{\cdot}2)\ \text{MHz} \qquad \text{theory: } (7315{\cdot}75 \pm 0{\cdot}02)\ \text{MHz}$$

The theoretical values are calculated by Erickson (1971) and their uncertainties are estimated for 68% confidence limits. As in part I, the experimental errors make due allowance for pressure shifts and current shifts and other systematic effects not yet examined in detail.

The value for the interval $S_{1/2}$–$D_{3/2}$ can be combined with the interval $S_{1/2}$–$P_{3/2}$ of $(20179{\cdot}7 \pm 1{\cdot}2)$ MHz measured by Jacobs *et al* (1971). This results in an experimental value for the Lamb shift $P_{3/2}$–$D_{3/2}$.

$$\Sigma_4(4^2P_{3/2}\text{–}4^2D_{3/2}) = (34{\cdot}4 \pm 9{\cdot}0)\ \text{MHz}$$

The two experimental errors have been added without consideration of the confidence levels. There is agreement with the theoretical value of $(\Sigma_4)_{\text{theor}} = (37{\cdot}19 \pm 1{\cdot}36)$ MHz from Erickson (1971 private communication).

We thank the Science Research Council for their support of this work.

References

Beyer H -J and Kleinpoppen
Eck T G and Huff R J 1968
pp 193–202
——1969 *Phys. Rev. Lett.* 22
Jacobs R R, Lea K R and L
Wieder H and Eck T G 1967

A cusp in low ene

D ANDR
Department
West Germa

MS received

Abstract. A
electron-sod
structure is

Theory (eg Mott and
open channel whenever
this effect depends on
known to be very stron
the alkali atoms, the la
phenomenon.

The experiment was
containing an electron
energetic halfwidth), a
about 5 mm above the
selection of the scatter
the electrons are counte
scaler. The detector ca

Some preliminary r
cross section as a functi

Shape and magnitud
results of Moores and
detected experimentally
the difference not only
the essential features ar
structure decreases up

The method recently described

References

Beyer H -J and Kleinpoppen H 1971 *J. Phys.* B: *Atom. molec. Phys.* **4** L129–32
Eck T G and Huff R J 1968 *Beam Foil Spectroscopy* ed. S Bashkin (New York: Gordon and Breach) pp 193–202
——1969 *Phys. Rev. Lett.* **22** 319–21
Jacobs R R, Lea K R and Lamb W E Jr 1971 *Phys. Rev.* A **3** 884–905
Wieder H and Eck T G 1967 *Phys. Rev.* **153** 103–12

A cusp in low energy electron–sodium scattering

D ANDRICK, M EYB and M HOFMANN

Department of Physics, University Trier-Kaiserslautern, D-675 Kaiserslautern, West Germany

MS received 23 November 1971

Abstract. A pronounced feature is observed in the differential cross section of elastic electron–sodium scattering. Shape and energetic position (2·1 eV) show, that the structure is due to the opening of the inelastic 3^2P-channel.

Theory (eg Mott and Massey 1971) predicts a structure in the cross section of an open channel whenever the threshold of a new channel is passed. The magnitude of this effect depends on the coupling between the channels. As this coupling is well known to be very strong between the ground state and the first excited (^2P) state of the alkali atoms, the latter are the most suitable targets for an investigation of this phenomenon.

The experiment was done in an apparatus previously described (Andrick *et al* 1968) containing an electron gun, which produces an energy selected beam (100 meV energetic halfwidth), a conventional alkali oven (beam pressure in the scattering centre about 5 mm above the oven 10^{-4} Torr) and a detector which again allows energy selection of the scattered electrons (60 meV halfwidth). Behind the energy analyser the electrons are counted by a multiplier; the pulses are stored in a 400 channel multiscaler. The detector can be rotated to cover an angular range from 0° to 145°.

Some preliminary results are shown in the figures. They show the differential cross section as a function of energy at various scattering angles.

Shape and magnitude of the structure are in quite good agreement with theoretical results of Moores and Norcross (1971 private communication). The structure as detected experimentally seems to be a little less pronounced than the calculated effect, the difference not only being a result of instrumental broadening. On the other hand the essential features are in full agreement: starting from small scattering angles the structure decreases up to about 60°, is enhanced then with a maximum between 90°

and 120° which is followed by a minimum around 130° and at last a new rise to higher angles. One might say, therefore, that the effect shows predominantly—though not exclusively—a d wave behaviour.

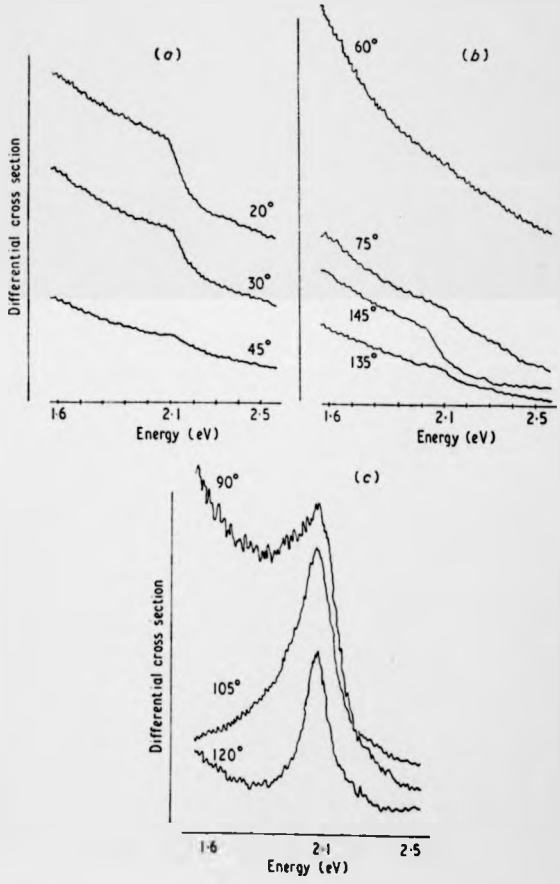

Figure 1. Differential cross section of elastic e^-–Na-scattering versus energy at various scattering angles. The scales of (*b*) and (*c*) are enlarged against the scale of (*a*) by a factor 3·7 and 25 respectively. The curves are calibrated against each other at 1·6 eV using theoretical data of Moores and Norcross (1971).

This is contradictory to what one would expect in a first order approximation assuming that in the inelastic 3^2P channel the scattering close to threshold takes place in the s wave only. The conclusion from this would be that as the target in its ground

Cascading Anticrossings from $n = 5$ He^+

H.-J. Beyer, H. Kleinpoppen, and J. M. Woolsey
Physics Department, University of Stirling, Stirling, Scotland
(Received 13 December 1971)

Electric-field-induced anticrossing signals of $n = 5$ He^+ are detected by intensity changes of the line He II 4686 Å ($n = 4$ to $n = 3$). The fine structure splittings $5^2S_{1/2}$-$5^2G_{1/2}$ and $5^2S_{1/2}$-$5^2G_{9/2}$ have been derived from the measurements to be 15 924.4 ± 5.9 and 17 040.5 ± 8.0 MHz, respectively, in agreement with the theoretical values of 15 920.0 and 17 043.6 MHz. The splitting $5^2G_{7/2}$-$5^2G_{9/2}$ is 1116.1 ± 14.0 MHz compared with the theoretical value of 1123.6 MHz.

Anticrossing signals in $n = 4$ of He^+ have been used recently to derive fine-structure intervals.[1,2] They are detected from intensity changes in the line complex 4686 Å ($n = 4$ to $n = 3$). However, the populations of the various $n = 4$ sublevels are not only changed by crossings occuring in $n = 4$, but also by the cascading effects of crossings occuring at higher n. Such effects, which are also present in rf investigations, usually lead to small asymmetries in the signal shape in precision fine-structure measurements.[3,4] In certain circumstances, however, they can be strong enough to be used to derive fine-structure splittings of a higher level. This is the case for anticrossings between $5S$ and $5G$, the subject of the present report.

The method recently described by Beyer and Kleinpoppen[2] for fine-structure splittings of $n = 4$ is employed here. Ions are produced by a low-current electron beam in about 10^{-2} Torr of helium. A magnetic field parallel to the beam causes a Zeeman splitting of the levels, and anticrossings are induced by a static electric field perpendicular to the magnetic field. The 4686-Å light from the region between the Stark plates is detected by a photomultiplier through a narrow-band interference filter. The small changes in the total signal are plotted as the magnetic field is swept through a level crossing. A simplified energy level diagram (Fig. 1) illustrates the detection process. The fraction of ions in the $5S$ state which decays with the emission of 4686 Å is very small, of the order of 1%, whereas all of the ions in $5G$ decay to $4F$ and then only to $3D$. Since

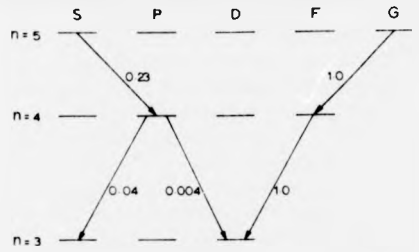

FIG. 1. Simplified energy-level diagram of He I. Only the branching ratios of interest in the present experiment are shown.

the lifetime of 5S is larger than that of 5G and 5S is also likely to be more populated by electron impact, an anticrossing between 5S and 5G magnetic sublevels results in a transfer of ions from 5S to 5G and a net increase in the 4686-Å signal. The observation of 4686 Å is particularly convenient, since polarizers and narrow-band interference filters are readily obtainable. This is not so for the lines from $n = 5$ which are at 10 124, 3203, 1085, and 237 Å.

Figure 2 shows some of the S and G levels in the magnetic field. The two anticrossings found to be strongest were $S_{1/2}{}^{1/2}$-$G_{7/2}{}^{-7/2}$ and $S_{1/2}{}^{1/2}$-$G_{9/2}{}^{-7/2}$ at calculated fields of 2409.73 and 2873.29 G, respectively. By measuring the positions of these anticrossings, using the Zeeman effect theory, the splittings in zero magnetic field can be derived. Theoretical values in this Letter have been obtained from the energy-level tables of Garcia and Mack,[5] which are truncated to allow for the effects of higher-order terms in the theoretical expression. Included in the Zeeman effect are corrections for the anomalous magnetic moment of the electron and the nuclear motion.

Resonance curves are almost pure absorption Lorentzian with amplitudes 1–2% of the total 4686-Å light. As a result of the lifetimes of the states involved, the curves are narrow, upwards from 6 G, depending on the strength of the electric field. A six-parameter Lorentzian fit has been made to about twenty data points taken from the curves to obtain the centers and widths more accurately.

Since the crossing point is shifted by the applied electric field, an extrapolation to zero electric field has been carried out. A least-squares fit has been made to all measured crossing points below 120 V cm^{-1} to obtain the intercept. Above this electric field there were obvious departures

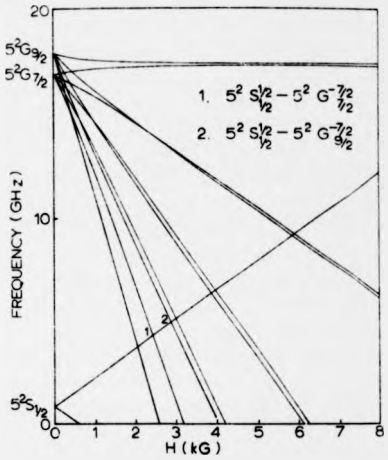

FIG. 2. Zeeman effect for the 5S and some of the 5G levels. The crossings used to determine the S–G splittings are labeled 1 and 2.

from the quadratic dependence. Figure 3 shows the experimental and theoretical Stark effect for the $S_{1/2}{}^{1/2}$-$G_{7/2}{}^{-7/2}$ crossing. The experimental intercept is 2410.46 G with a standard deviation of 0.17 G. For the $S_{1/2}{}^{1/2}$-$G_{9/2}{}^{-7/2}$ crossing there is closer agreement between experiment and theory, the intercept of the extrapolation being 2872.73 G

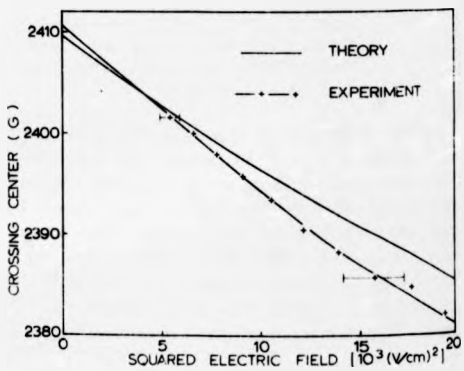

FIG. 3. Experimental and theoretical crossing points for $S_{1/2}{}^{1/2}$-$G_{7/2}{}^{-7/2}$ as a function of the squared electric field. The Stark shifts were calculated as a perturbation of the level system given by the magnetic field. The error shown is due to a 5% uncertainty in the distance between the Stark plates in this initial experimental setup.

with a standard deviation 0.29 G. In order to take account of systematic effects which have not yet been fully investigated, for example, pressure and electron current shifts, errors for the crossings are quoted as 0.8 G and 1.5 G, respectively. Using the theory of the Zeeman effect, the splittings $S_{1/2}$-$G_{7/2}$ and $S_{1/2}$-$G_{9/2}$ in zero magnetic field are found to be 15924.4 ± 5.9 and 17040.5 ± 8.0 MHz, respectively. From these a value of 1116.1 ± 14.0 MHz for $G_{7/2}$-$G_{9/2}$ is deduced, in agreement with the theoretical splitting of 1123.6 MHz.

We gratefully acknowledge the support given by the Science Research Council.

[1]T. G. Eck and R. J. Huff, in *Beam Foil Spectroscopy*, edited by S. Baskin (Gordon and Breach, New York, 1968), p. 193, and Phys. Rev. Lett. 22, 319 (1969).

[2]H.-J. Beyer and H. Kleinpoppen, J. Phys. B: Proc. Phys. Soc., London 4, L129 (1971).

[3]R. R. Jacobs, K. R. Lea, and W. E. Lamb, Jr., Phys. Rev. A 3, 884 (1971).

[4]D. L. Mader, M. Leventhal, and W. E. Lamb, Jr., Phys. Rev. A 3, 1832 (1971).

[5]J. D. Garcia and J. E. Mack, J. Opt. Soc. Amer. 55, 654 (1965).